



Spatio-temporal modelling of the NF- κ B intracellular signalling pathway: The roles of diffusion, active transport, and cell geometry

Alan J. Terry*, Mark A.J. Chaplain

Division of Mathematics, University of Dundee, Dundee, Scotland DD1 4HN, UK

ARTICLE INFO

Article history:

Received 25 February 2011

Received in revised form

1 July 2011

Accepted 27 August 2011

Available online 5 September 2011

Keywords:

NF- κ B

Spatio-temporal model

Diffusion

Active transport

Cell geometry

ABSTRACT

The nuclear factor kappa B (NF- κ B) intracellular signalling pathway is central to many stressful, inflammatory, and innate immune responses. NF- κ B proteins themselves are transcription factors for hundreds of genes. Experiments have shown that the NF- κ B pathway can exhibit oscillatory dynamics—a negative feedback loop causes oscillatory nuclear-cytoplasmic translocation of NF- κ B. Given that cell size and shape are known to influence intracellular signal transduction, we consider a spatio-temporal model of partial differential equations for the NF- κ B pathway, where we model molecular movement by diffusion and, for several key species including NF- κ B, by active transport as well.

Through numerical simulations we find values for model parameters such that sustained oscillatory dynamics occur. Our spatial profiles and animations bear a striking resemblance to experimental images and movie clips employing fluorescent fusion proteins. We discover that oscillations in nuclear NF- κ B may occur when active transport is across the nuclear membrane only, or when no species are subject to active transport. However, when active transport is across the nuclear membrane and NF- κ B is additionally actively transported through the cytoplasm, oscillations are lost. Hence transport mechanisms in a cell will influence its response to activation of its NF- κ B pathway. We also demonstrate that sustained oscillations in nuclear NF- κ B are somewhat robust to changes in the shape of the cell, or the shape, location, and size of its nucleus, or the location of ribosomes. Yet if the cell is particularly flat or the nucleus sufficiently small, then oscillations are lost. Thus the geometry of a cell may partly determine its response to NF- κ B activation.

The NF- κ B pathway is known to be constitutively active in several human cancers. Our spatially explicit modelling approach will allow us, in future work, to investigate targeted drug therapy of tumours.

© 2011 Elsevier Ltd. All rights reserved.

1. Introduction

Various intracellular signalling pathways are known to exhibit oscillatory dynamics. Examples include the Hes1 (Hirata et al., 2002; Bernard et al., 2006), Wnt (Dequeant et al., 2006; Wawra et al., 2007), p53 (Bar-Or et al., 2000; Lahav et al., 2004), and nuclear factor kappa B (NF- κ B) pathways (Nelson et al., 2004; Krishna et al., 2006; Friedrichsen et al., 2006). The purpose of oscillatory dynamics depends on the context in which it arises but, at least for the pathways just listed, the underlying mechanism is believed to depend on a negative feedback loop (Monk, 2003; Pigolotti et al., 2007; Tiana et al., 2007; Gordon et al., 2009). There have been many studies of the temporal behaviour of these pathways (Nelson et al., 2004; Monk, 2003; Kruger and Heinrich,

2004; Hoffmann et al., 2002) but comparatively few studies of their spatio-temporal behaviour (Gordon et al., 2009; Sturrock et al., 2011). Yet there is experimental evidence suggesting that cell size and shape can significantly influence intracellular signal transduction (Meyers et al., 2006; Neves et al., 2008). Moreover, the spatial distribution of molecules is clearly of relevance to their pattern of interaction. Such reasoning indicates that it would be a progressive step in the computational modelling of intracellular signalling pathways if more spatio-temporal models were to be created and explored.

Spatio-temporal models accounting for diffusion and spatial properties such as the location of ribosomes have recently appeared for Hes1 (Sturrock et al., 2011), p53 (Gordon et al., 2009; Sturrock et al., 2011), and Notch-Delta signalling (Terry et al., 2011). However, we are not aware of any such attempt to examine NF- κ B, despite the fact that there are now a substantial number of papers on the temporal modelling of NF- κ B (Nelson et al., 2004; Krishna et al., 2006; Hoffmann et al., 2002; Cheong

* Corresponding author.

E-mail address: aterry@maths.dundee.ac.uk (A.J. Terry).

et al., 2008; Lipniacki et al., 2004; Ashall et al., 2009; Hat et al., 2009). Hence our purpose here will be to explore a spatio-temporal model of the NF- κ B pathway. Our model will be a system of partial differential equations in which the movement of molecules by diffusion will be explicitly considered. The movement by active transport of several key species, including NF- κ B itself, will also be considered.

The value of modelling NF- κ B is clear when one bears in mind its many biological roles. NF- κ B proteins are present in most animal cells and are central to many stressful, inflammatory, and innate immune responses (Krishna et al., 2006; Alberts et al., 2008). Normally NF- κ B is held functionally inert in the cytoplasm by Inhibitor of kappa B ($\text{I}\kappa\text{B}$) proteins. There are a number of isoforms of $\text{I}\kappa\text{B}$, including $\text{I}\kappa\text{B}\alpha$, $\text{I}\kappa\text{B}\beta$, and $\text{I}\kappa\text{B}\epsilon$ (Lipniacki et al., 2004). In response to signals originating from a diverse array of sources, $\text{I}\kappa\text{B}$ becomes phosphorylated and thereby tagged for rapid destruction (Alberts et al., 2008). As a result, NF- κ B is liberated from $\text{I}\kappa\text{B}$ and translocates to the nucleus where it acts as a transcription factor for several hundred genes, one of which is the gene for $\text{I}\kappa\text{B}\alpha$ (Alberts et al., 2008; Lipniacki et al., 2004; Ashall et al., 2009). Newly synthesised $\text{I}\kappa\text{B}\alpha$ binds to the liberated NF- κ B, causing NF- κ B to again be sequestered in the cytoplasm (Alberts et al., 2008; Weinberg, 2007). In the presence of a sustained signal, NF- κ B is again liberated and the process just described repeats. Consequently, oscillations in liberated or “free” NF- κ B and $\text{I}\kappa\text{B}\alpha$ can occur, as revealed experimentally (see Nelson et al., 2004; Friedrichsen et al., 2006; Ashall et al., 2009 and Fig. 1). The interactions of NF- κ B and $\text{I}\kappa\text{B}\alpha$ in the presence of a continuous signal form a negative feedback loop (Alberts et al., 2008, Fig. 15–80(A)).

The NF- κ B pathway is not only regulated by $\text{I}\kappa\text{B}$ proteins. NF- κ B induces transcription of the protein A20, whilst A20 is known to inhibit the mechanism by which $\text{I}\kappa\text{B}$ proteins are degraded in the presence of a signal (Lee et al., 2000; Lipniacki et al., 2004; Song et al., 1996). Since A20 attenuates $\text{I}\kappa\text{B}$ degradation, it enhances the capacity of $\text{I}\kappa\text{B}$ to sequester NF- κ B.

Some genes are only switched on by NF- κ B after it has been active for several hours (Hoffmann et al., 2002). This suggests that its oscillatory behaviour may have a functional significance. However, the purpose and implications of this behaviour is not yet fully understood (Krishna et al., 2006; Ashall et al., 2009).

Genes activated by NF- κ B include those whose protein products possess anti-apoptotic properties, such as Bcl-1, IAP-1, and IAP-2 (Weinberg, 2007). NF- κ B can also function in a mitogenic fashion by inducing expression of genes that form part of the cell cycle machinery, such as the *myc* and cyclin D1 genes (Weinberg, 2007). Hence NF- κ B can protect cells from apoptosis and can drive their proliferation. Consequently, if the machinery in a cell becomes deregulated in such a way as to leave the NF- κ B

pathway constitutively active, then the cell has greater potential to turn cancerous. Indeed the NF- κ B pathway has been found to be constitutively active in a number of types of human tumour, including B- and T-cell lymphomas, myelomas, and cervical carcinomas (Nair et al., 2003; Kokura et al., 2005). Blocking of the NF- κ B pathway has been seen to suppress tumour incidence (Kokura et al., 2005; Chang et al., 2007; Park et al., 2009). This blocking can be achieved by different means (Kokura et al., 2005; Chang et al., 2007; Park et al., 2009). We anticipate that spatio-temporal modelling may shed light on targeted drug therapy and suggest directions for improving the efficacy of treatment strategies. However, since this work is an initial effort to explore spatial effects in the NF- κ B pathway, our analysis will be based on a reduced description of the pathway that demonstrates cyclic behaviour and we defer a more detailed analysis with targeted drug therapy to a future study.

This paper is organised as follows. In Section 2 we outline the biological mechanism of the NF- κ B pathway. We convert this mechanism into a mathematical model in Section 3. This model is non-dimensionalised in Section 4. We numerically explore the non-dimensionalised model in Section 5. This allows us to find dimensional parameter values that yield sustained oscillatory dynamics. For rates of diffusion, active transport, and degradation, we find ranges of values such that oscillatory behaviour persists. In Section 5.1, we discuss temporal plots and spatial profiles when the cell is circular, noting in particular that our spatial profiles demonstrate behaviour strikingly similar to the experimental results in Fig. 1. We note also that oscillations in nuclear NF- κ B may occur when all active transport rates are set equal to zero, so that molecular transport is by diffusion alone, though this causes less NF- κ B to enter the nucleus. In Section 5.2, we explore the robustness of sustained oscillations in nuclear NF- κ B to changes in the geometry of the cell. We vary the shape of the cell, the shape, location, and size of its nucleus, and the location of ribosomes, finding that oscillations are robust to this variation up to a point. Oscillations are lost when the nucleus is significantly reduced in size, when the cell is especially flat, or when protein translation in ribosomes occurs suitably far from the nucleus. We are led to speculate that the geometry of a cell may partly determine its response to NF- κ B activation. We draw conclusions and consider ways to extend our work in Section 6. Animations are included as Supporting Information files.

2. Kinetics of the NF- κ B pathway

We have already touched upon the kinetics of the NF- κ B pathway in the Introduction. Now we discuss these kinetics in more detail. Our discussion will be based on the interactions

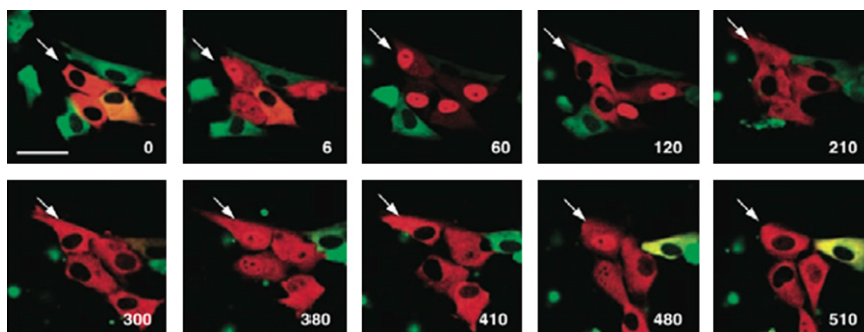


Fig. 1. Experimental observation of oscillations in NF- κ B localisation. This figure shows time-lapse confocal images of NF- κ B-containing species fused to a red fluorescent protein and of $\text{I}\kappa\text{B}\alpha$ -containing species fused to a green fluorescent protein in SK-N-AS cells after stimulation with TNF α . The arrow marks one oscillating cell. Nuclear-cytoplasmic translocation of NF- κ B-containing species is apparent. Time is shown in minutes and the scale bar represents 50 μm . Reproduced with copyright permission from Fig. 1B in Nelson et al. (2004). (For interpretation of the references to colour in this figure legend, the reader is referred to the web version of this article.)

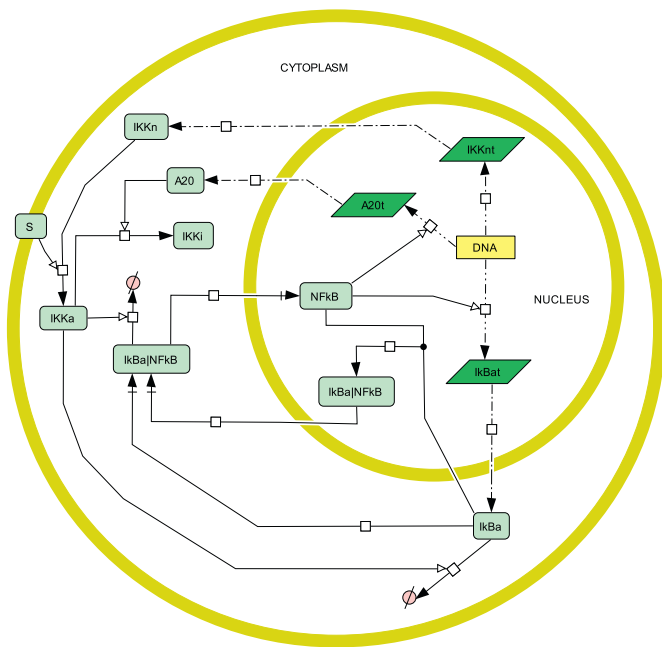


Fig. 2. Cell circuitry schematic of the NF- κ B signalling pathway. IKK α transcript (shown as IKKnt) is transcribed in the nucleus. It diffuses to the cytoplasm and creates IKK α by translation. The species S represents a generic signalling cascade that activates IKK α , converting it to IKKa. IKKa mediates degradation of free I κ B α and of I κ B α in the complex I κ B α |NF κ B. This latter reaction liberates NF- κ B, which translocates to the nucleus and mediates production of I κ B α transcript (shown as I κ Bat) and A20 transcript (shown as A20t). I κ B α transcript and A20 transcript diffuse to the cytoplasm and respectively create I κ B α and A20 by translation. Newly synthesised I κ B α binds to NF- κ B in the nucleus and cytoplasm and sequesters it in the cytoplasm in the complex I κ B α |NF κ B. At the same time, newly synthesised A20 deactivates IKKa, converting it to IKKi. In the presence of a sustained signal, the process just described repeats, leading to oscillations in NF- κ B in both time and space. Some reactions shown here involve intermediate species that are not depicted.

presented in the cell circuitry schematic in Fig. 2. Extracellular stimuli that activate the NF- κ B pathway include bacteria, viruses, interleukin-1, and tumour necrosis factor- α (TNF α) (Alberts et al., 2008; Weinberg, 2007). Many recent experimental and computational studies have taken TNF α to be the external stimulus (see Cheong et al., 2008 and references therein). In Fig. 2 we represent the extracellular stimulus as a generic signalling molecule or cascade, which we denote S.

Extracellular stimuli activate the NF- κ B pathway by triggering a chain of reactions that results in the phosphorylation of I κ B kinase (IKK) (Nelson et al., 2004). The phosphorylation of IKK converts it from a neutral form (IKK α) to an active form (IKKa) (Lipniacki et al., 2004). The signalling cascade that leads to the phosphorylation of IKK varies according to the stimulus but the outcome is the same (Alberts et al., 2008). Since our interest is in a simplified description that permits spatial insight into NF- κ B oscillations, we shall model IKK activation by assuming that, in the presence of a sustained continuous signal, IKKa appears at a constant rate in the outer cytoplasm. We also assume that IKKa degrades naturally, is deactivated (that is, converted to an inactive form IKKi) both spontaneously and by the protein A20, and does not enter the nucleus, all of which is in keeping with previous models (Lipniacki et al., 2004; Puszyński et al., 2009). A thorough consideration of IKK activation may be found in a recent paper by Werner et al. (2008).

As mentioned in the Introduction, NF- κ B is usually sequestered in the cytoplasm by association with I κ B proteins. Activated IKK (IKKa) phosphorylates I κ B (whether it is bound to NF- κ B or unbound), which tags I κ B for rapid destruction. The destruction

of I κ B that is bound to NF- κ B liberates the NF- κ B, which translocates to the nucleus and initiates the transcription of its target genes (Fig. 2). Most of the I κ B-family inhibition of NF- κ B is carried out by the isoform I κ B α (Cheong et al., 2008; Lipniacki et al., 2004; Sun et al., 1993). In cells lacking other isoforms (I κ B β , I κ B ϵ), pronounced oscillations have been observed (Hoffmann et al., 2002; Cheong et al., 2008). The role of I κ B β and I κ B ϵ isoforms seems to be to dampen these oscillations (Hoffmann et al., 2002; Cheong et al., 2008). As in a number of other studies (Krishna et al., 2006; Lipniacki et al., 2004), we shall only include the I κ B α isoform in our model, so that it will make sense to seek values for the model parameters such that stable oscillations occur.

One of the genes targeted by the transcription factor NF- κ B is the gene for I κ B α . We will model this by assuming that I κ B α transcript is produced in the nucleus as a saturating function of NF- κ B concentration in the nucleus. A saturating function is sensible because every gene type has only a small number of copies. Typically there are only two copies (Puszyński et al., 2009; Ashall et al., 2009) but there can be more (Schridder and Hahn, 2010) and in particular gene copy number is known to be elevated (or “amplified”) in certain forms of cancer (Chung et al., 2006). Mathematical models in which NF- κ B-induced production of I κ B α transcript is not saturating but grows as a linear, quadratic, or even cubic power of NF- κ B have predicted that the oscillatory period of the pathway is a rapidly growing function of total NF- κ B, which is in disagreement with experiments (Hat et al., 2009). We further assume that I κ B α transcript diffuses out into the cytoplasm where it produces I κ B α by translation. Newly synthesised I κ B α moves into the nucleus, binds to NF- κ B, and leads it out into the cytoplasm where it is again sequestered (Lipniacki et al., 2004), completing a negative feedback loop.

To facilitate their function, transcription factors may not simply diffuse into the nucleus but may also be actively transported (Arenzana-Seisdedos et al., 1997; Mackenzie et al., 2006; Lomakin and Nadezhkina, 2010). Hence we assume in our model that nuclear translocation of NF- κ B occurs both by diffusion and active transport. Given that newly synthesised I κ B α binds to nuclear NF- κ B and sequesters it in the cytoplasm, we assume that I κ B α can both diffuse and be actively transported into the nucleus, and that the complex of I κ B α bound to NF- κ B (which we denote I κ B α |NF κ B) can both diffuse and be actively transported out of the nucleus.

The gene for A20 is, like the gene for I κ B α , a target for NF- κ B. Hence, as we did for I κ B α transcript, we assume that A20 transcript is produced in the nucleus as a saturating function of NF- κ B. A20 transcript diffuses into the cytoplasm where it produces A20 protein by translation and A20 protein contributes to IKKa deactivation, as mentioned above.

As in many previous studies (Nelson et al., 2004; Hoffmann et al., 2002; Cheong et al., 2008; Lipniacki et al., 2004), we suppose that the total amount of NF- κ B-containing complexes is constant. Hence these complexes will not be subject to natural degradation. On the other hand, IKKa, I κ B α transcript, I κ B α , A20 transcript, and A20 will be subject to such degradation.

Our modelling assumptions are incomplete without initial conditions. We suppose, as in Hoffmann et al. (2002) and Lipniacki et al. (2004), that the initial concentrations of all species are zero, except for I κ B α |NF κ B which is positive everywhere in the cytoplasm, in keeping with the discussion above.

3. Mathematical model

We now present a mathematical model based on the assumptions discussed in the previous section. We describe our ideas in

more or less the same order as the corresponding biological assumptions in the last section. Our modelling assumptions are similar to those in Lipniacki et al. (2004) with the following differences: we model molecular movement by diffusion and active transport, we model the signalling cascade that activates IKK in slightly less detail, and (as in Ashall et al., 2009) we represent NF- κ B-inducible transcription as a saturating function of NF- κ B rather than as a less realistic linear function. There are three compartments in our model—the cytoplasm, nuclear membrane, and nucleus. The equations for our model are different in the different compartments. Our model will be a system of partial differential equations (PDEs) with two independent spatial variables, x and y . We define dependent variables as follows:

- $[IKKa(x,y,t)]$, $[IKKa|IkBz(x,y,t)]$, and $[IKKa|IkBz|NFkB(x,y,t)]$ are the concentrations at time t at the point (x,y) in the cell of, respectively, active IKK (IKKa), the complex of IKKa and IkBz ($IKKa|IkBz$), and the complex of IKKa and IkBz|NFkB ($IKKa|IkBz|NFkB$),
- $[IkBz|NFkB(x,y,t)]$ and $[NFkB(x,y,t)]$ are the concentrations at time t at the point (x,y) in the cell of, respectively, the complex of IkBz and NF- κ B ($IkBz|NFkB$) and free NF- κ B,
- $[IkBz_t(x,y,t)]$, $[IkBz(x,y,t)]$, $[A20_t(x,y,t)]$, and $[A20(x,y,t)]$ are the concentrations at time t at the point (x,y) in the cell of, respectively, IkBz transcript, IkBz protein, A20 transcript, and A20 protein.

The subscript “ t ” denoting “transcript” in $[IkBz_t(x,y,t)]$ and $[A20_t(x,y,t)]$ is not to be confused with the independent time variable t . In fact, for ease of notation, we omit unnecessary reference to the independent variables henceforth. Thus, for example, we will refer to $[IkBz_t(x,y,t)]$ and $[A20_t(x,y,t)]$ simply as $[IkBz_t]$ and $[A20_t]$, and so on.

Our model contains many parameters, so a transparent notation system for them is sensible. In what follows, the letters A , B , C , d , D , and E will respectively refer to rates of association, transcription, catalytic degradation, natural (that is, not catalytic) degradation, diffusion, and translation. Subscripts will be attached to parameters where this is needed to distinguish between different species or reactions. Additionally, the names and concise description of all the parameters are given in Table 1 below.

We conduct our simulations from time $t=0$ onwards. To allow the resting cell to reach an equilibrium state prior to stimulation, we assume that continuous stimulation begins at a positive time T . A similar assumption has been used in other models of the NF- κ B pathway (Lipniacki et al., 2004).

In our model, IKKa is present only in the cytoplasm. We assume that the effect of continuous cell stimulation is to cause activation of IKK in the outer cytoplasm. Hence from time $T > 0$ onwards we assume that IKKa appears at a constant rate F in the outer cytoplasm, specifically within a distance H_1 of the cell membrane. This assumption is reasonable because, whilst many kinases are activated right at the cell membrane (Kholodenko, 2006), some may be activated further into the cell, which is true in particular of IKK (Lipniacki et al., 2004; Werner et al., 2008). We suppose that IKKa diffuses with diffusion coefficient D_{IKKa} , degrades at a per molecule rate d_{IKKa} , and is spontaneously deactivated at a per molecule rate G . It is deactivated by A20 after the onset of continuous cell stimulation, which occurs at a mass action rate proportional to the concentrations of IKKa and A20 with rate parameter J . IKKa forms complexes with IkBz at a rate proportional to the concentrations of IKKa and IkBz with constant of proportionality or association rate A_1 . Similarly it forms complexes with IkBz|NFkB with association rate A_2 . These complexes are formed because IKKa catalytically degrades free

Table 1

Definitions and values of parameters in the model of Eqs. (1)–(19). Here X represents any of the species in the model, Y represents IKKa, IkBz transcript, IkBz, A20 transcript, and A20, and Z represents IkBz|NFkB, NF- κ B, and IkBz.

Parameter	Definition	Value
D_X	Diffusion coefficient of species X	$0.0425 \mu\text{m}^2 \text{s}^{-1}$
d_Y	Degradation rate of species Y	0.00100s^{-1}
a_Z	Active transport rate of species Z	$0.438 \mu\text{m} \text{s}^{-1}$
A_1	Association of IKKa and IkBz	$0.375(\mu\text{M})^{-1} \text{s}^{-1}$
A_2	Association of IKKa and IkBz NFkB	$0.750(\mu\text{M})^{-1} \text{s}^{-1}$
A_3	Association of IkBz and NF- κ B	$0.375(\mu\text{M})^{-1} \text{s}^{-1}$
B_1	Maximal NF- κ B-inducible production of IkBz transcript	$0.0000128 \mu\text{M} \text{s}^{-1}$
B_2	Maximal NF- κ B-inducible production of A20 transcript	$0.0000128 \mu\text{M} \text{s}^{-1}$
C_1	IKKa IkBz catalysis	0.0300s^{-1}
C_2	IKKa IkBz NFkB catalysis	0.0600s^{-1}
E_1	IkBz translation	0.0750s^{-1}
E_2	A20 translation	0.0750s^{-1}
F	Appearance of IKKa in outer cytoplasm	$0.000320 \text{M} \text{s}^{-1}$
G	Spontaneous deactivation of IKKa	0.003s^{-1}
h	NF- κ B-inducible transcription Hill coefficient	2
H_1	Maximum distance of IKK activation from cell membrane	$2.92 \mu\text{m}$
H_2	Minimum distance of translation from nuclear membrane	$2.92 \mu\text{m}$
J	IKKa inactivation by A20	$1.25(\mu\text{M})^{-1} \text{s}^{-1}$
K	Natural degradation of IkBz in IkBz NFkB	0.00000600s^{-1}
M	NF- κ B concentration at which NF- κ B-inducible transcription is half-maximal	$0.0052 \mu\text{M}$

IkBz and IkBz in IkBz|NFkB. Catalytic degradation of these complexes, at rates C_1 and C_2 respectively, releases IKKa. We arrive at the following PDE:

$$\begin{aligned} \frac{\partial [IKKa]}{\partial t} = & D_{IKKa} \nabla^2 [IKKa] + \gamma_t \phi_{r_1} F - G [IKKa] - \gamma_t J [IKKa] [A20] \\ & - A_1 [IKKa] [IkBz] - A_2 [IKKa] [IkBz] [NFkB] + C_1 [IKKa] [IkBz] \\ & + C_2 [IKKa] [IkBz] [NFkB] - d_{IKKa} [IKKa], \end{aligned} \quad (1)$$

where γ_t represent a Heaviside function of t such that $\gamma_t = 0$ if $t < T$ and $\gamma_t = 1$ if $t \geq T$, and where ϕ_{r_1} is a Heaviside function of x and y defined as follows: at the point (x,y) in the cytoplasm, $\phi_{r_1} = 1$ if the distance r_1 of (x,y) from the cell membrane is less than or equal to H_1 and otherwise $\phi_{r_1} = 0$.

The complex $IKKa|IkBz$ is present only in the cytoplasm. It diffuses at rate $D_{IKKa|IkBz}$. As we saw in the last paragraph, it is formed when IKKa binds to IkBz with binding rate parameter A_1 and it dissociates at a per molecule rate C_1 . Thus we have:

$$\begin{aligned} \frac{\partial [IKKa|IkBz]}{\partial t} = & D_{IKKa|IkBz} \nabla^2 [IKKa|IkBz] \\ & + A_1 [IKKa] [IkBz] - C_1 [IKKa|IkBz]. \end{aligned} \quad (2)$$

The complex $IKKa|IkBz|NFkB$ is present only in the cytoplasm where it diffuses at rate $D_{IKKa|IkBz|NFkB}$. It is formed when IKKa binds to IkBz|NFkB in order to catalytically degrade the IkBz in IkBz|NFkB. Association of IKKa and IkBz|NFkB has binding rate parameter A_2 . Catalytic activity of IKKa causes $IKKa|IkBz|NFkB$ to dissociate at a per molecule rate C_2 , releasing IKKa and liberating NF- κ B. In summary, we can write

$$\begin{aligned} \frac{\partial [IKKa|IkBz|NFkB]}{\partial t} = & D_{IKKa|IkBz|NFkB} \nabla^2 [IKKa|IkBz|NFkB] \\ & + A_2 [IKKa] [IkBz] [NFkB] - C_2 [IKKa|IkBz|NFkB]. \end{aligned} \quad (3)$$

The complex $IkBz|NFkB$ may be present in both the cytoplasm and the nucleus, and may travel between these regions across the nuclear membrane. In the cytoplasm, it diffuses at rate $D_{IkBz|NFkB}$ and is formed when IkBz binds to NF- κ B with rate parameter A_3 .

It is lost when IKKa binds to it in order to catalytically degrade $I\kappa B\alpha$. This binding occurs with rate parameter A_2 . We also assume $I\kappa B\alpha|NF\kappa B$ dissociates at a rate K due to natural degradation of the $I\kappa B\alpha$ in it, which liberates $NF\kappa B$. Hence we find in the cytoplasm that

$$\frac{\partial[I\kappa B\alpha|NF\kappa B]}{\partial t} = D_{I\kappa B\alpha|NF\kappa B} \nabla^2 [I\kappa B\alpha|NF\kappa B] + A_3 [I\kappa B\alpha][NF\kappa B] - A_2 [IKKa][I\kappa B\alpha|NF\kappa B] - K [I\kappa B\alpha|NF\kappa B]. \quad (4)$$

Our PDE for $I\kappa B\alpha|NF\kappa B$ in the nucleus is different from the cytoplasm in two respects. Firstly, IKKa does not bind to $I\kappa B\alpha|NF\kappa B$ in the nucleus since IKKa is not present there. Secondly, we no longer assume $I\kappa B\alpha|NF\kappa B$ dissociates due to natural degradation of the $I\kappa B\alpha$ in it, as in Lipniacki et al. (2004). Thus we find in the nucleus that

$$\frac{\partial[I\kappa B\alpha|NF\kappa B]}{\partial t} = D_{I\kappa B\alpha|NF\kappa B} \nabla^2 [I\kappa B\alpha|NF\kappa B] + A_3 [I\kappa B\alpha][NF\kappa B]. \quad (5)$$

In the nuclear membrane compartment, we suppose that $I\kappa B\alpha|NF\kappa B$ diffuses and does not form complexes with other species or dissociate. It is also actively transported (that is, convected) outwards, towards the cytoplasm, an assumption consistent with the experimental observation that it has a nuclear export sequence (Arenzana-Seisdedos et al., 1997). This assumption is modelled using a vector $\mathbf{a}_{I\kappa B\alpha|NF\kappa B}$ with constant magnitude or speed $a_{I\kappa B\alpha|NF\kappa B}$ that is directed away from the point $(x, y) = (0, 0)$. In a nucleus with centre $(0, 0)$, active transport will then be in directions radially outwards from the centre towards the cytoplasm. Biologically, our active transport assumption represents facilitated transport through nuclear pore complexes. In summary, we can write

$$\frac{\partial[I\kappa B\alpha|NF\kappa B]}{\partial t} = D_{I\kappa B\alpha|NF\kappa B} \nabla^2 [I\kappa B\alpha|NF\kappa B] - \nabla \cdot ([I\kappa B\alpha|NF\kappa B] \mathbf{a}_{I\kappa B\alpha|NF\kappa B}). \quad (6)$$

The vector $\mathbf{a}_{I\kappa B\alpha|NF\kappa B}$ may be written explicitly as

$$\left(\frac{a_{I\kappa B\alpha|NF\kappa B} x}{\sqrt{x^2 + y^2}}, \frac{a_{I\kappa B\alpha|NF\kappa B} y}{\sqrt{x^2 + y^2}} \right).$$

$NF\kappa B$ may be present in the cytoplasm, nucleus, or nuclear membrane. In the cytoplasm it diffuses at rate $D_{NF\kappa B}$ and is lost when $I\kappa B\alpha$ binds to it with rate parameter A_3 . It appears where the complex $I\kappa B\alpha|NF\kappa B$ dissociates at a rate K due to natural degradation of the $I\kappa B\alpha$ in this complex, which liberates $NF\kappa B$ (see (4)). It additionally appears where IKKa catalytically degrades $I\kappa B\alpha$ in $I\kappa B\alpha|NF\kappa B$ since this degradation also liberates $NF\kappa B$. As we mentioned in describing (3), this degradation is modelled as dissociation of $IKKa|I\kappa B\alpha|NF\kappa B$ with rate parameter C_2 . Our assumptions yield the following PDE for $NF\kappa B$ in the cytoplasm:

$$\frac{\partial[NF\kappa B]}{\partial t} = D_{NF\kappa B} \nabla^2 [NF\kappa B] - A_3 [I\kappa B\alpha][NF\kappa B] + C_2 [IKKa][I\kappa B\alpha|NF\kappa B] + K [I\kappa B\alpha|NF\kappa B]. \quad (7)$$

In the nucleus, $NF\kappa B$ diffuses and is lost when $I\kappa B\alpha$ binds to it. However it is not liberated from $I\kappa B\alpha$ because this liberation is assumed to occur only in the cytoplasm. Hence nuclear $NF\kappa B$ satisfies

$$\frac{\partial[NF\kappa B]}{\partial t} = D_{NF\kappa B} \nabla^2 [NF\kappa B] - A_3 [I\kappa B\alpha][NF\kappa B]. \quad (8)$$

Across the nuclear membrane, we suppose that $NF\kappa B$ diffuses. $NF\kappa B$ is a transcription factor which must travel to the nucleus to fulfil its transcriptional role and it is known to possess a nuclear localisation sequence which is masked when $I\kappa B\alpha$ binds to it (Mackenzie et al., 2006; Mikenberg et al., 2007). Hence we also suppose that $NF\kappa B$ is actively transported (convected) towards

the nucleus. As in the paragraph before Eq. (6), our active transport assumption implicitly takes the nucleus to be centred at $(x, y) = (0, 0)$ though now the active transport is directed straight towards the nucleus instead of straight out of it and is represented by a velocity vector $\mathbf{a}_{NF\kappa B}$ with constant magnitude or speed $a_{NF\kappa B}$. Our considerations lead to

$$\frac{\partial[NF\kappa B]}{\partial t} = D_{NF\kappa B} \nabla^2 [NF\kappa B] + \nabla \cdot ([NF\kappa B] \mathbf{a}_{NF\kappa B}). \quad (9)$$

We assume $I\kappa B\alpha$ transcript diffuses at rate $D_{I\kappa B\alpha}$ and degrades at rate $d_{I\kappa B\alpha}$ in the cytoplasm, which yields

$$\frac{\partial[I\kappa B\alpha_t]}{\partial t} = D_{I\kappa B\alpha} \nabla^2 [I\kappa B\alpha_t] - d_{I\kappa B\alpha} [I\kappa B\alpha_t]. \quad (10)$$

In the nucleus, we suppose that $I\kappa B\alpha$ transcript diffuses and degrades at the same rates as in the cytoplasm. We also suppose that it is produced by transcription as a saturating function of $NF\kappa B$, in keeping with our earlier discussion of transcription in Section 2. To be specific, the transcription rate is proportional (with constant of proportionality B_1) to a Hill function with Hill coefficient h and half-maximal rate M , as in Ashall et al. (2009). Hence in the nucleus, we have

$$\frac{\partial[I\kappa B\alpha_t]}{\partial t} = D_{I\kappa B\alpha} \nabla^2 [I\kappa B\alpha_t] + B_1 \left(\frac{[NF\kappa B]^h}{[NF\kappa B]^h + M^h} \right) - d_{I\kappa B\alpha} [I\kappa B\alpha_t]. \quad (11)$$

Across the nuclear membrane, $I\kappa B\alpha$ transcript diffuses

$$\frac{\partial[I\kappa B\alpha_t]}{\partial t} = D_{I\kappa B\alpha} \nabla^2 [I\kappa B\alpha_t]. \quad (12)$$

We assume $I\kappa B\alpha$ diffuses at rate $D_{I\kappa B\alpha}$ and degrades at rate $d_{I\kappa B\alpha}$ in the cytoplasm. It is translated from $I\kappa B\alpha$ transcript at a per molecule rate E_1 . Proteins are translated from mRNA by ribosomes in the cytoplasm, a process that is likely to occur at least some minimal distance from the nuclear membrane, so we assume that $I\kappa B\alpha$ is translated some minimal distance H_2 from the nuclear membrane. An assumption of this kind is also made in two recent studies that are similar in scope to this work (Terry et al., 2011; Sturrock et al., 2011). $I\kappa B\alpha$ is lost when it combines with and sequesters $NF\kappa B$ with rate parameter A_3 . It is also lost when IKKa binds to it with rate parameter A_1 , a reaction that occurs because IKKa catalytically degrades $I\kappa B\alpha$. Combining our assumptions yields a PDE for $I\kappa B\alpha$ in the cytoplasm:

$$\frac{\partial[I\kappa B\alpha]}{\partial t} = D_{I\kappa B\alpha} \nabla^2 [I\kappa B\alpha] + \theta_{r_2} E_1 [I\kappa B\alpha_t] - A_1 [IKKa][I\kappa B\alpha] - A_3 [I\kappa B\alpha][NF\kappa B] - d_{I\kappa B\alpha} [I\kappa B\alpha], \quad (13)$$

where θ_{r_2} is a Heaviside function of x and y defined as follows: at the point (x, y) in the cytoplasm, $\theta_{r_2} = 0$ if the distance r_2 of (x, y) from the nuclear membrane is less than H_2 and otherwise $\theta_{r_2} = 1$.

In the nucleus we assume $I\kappa B\alpha$ diffuses and degrades at the same rates as in the cytoplasm. It is also lost when it binds to and sequesters $NF\kappa B$ with rate parameter A_3 . But it is not subject to the other processes described in (13) since these are specific to the cytoplasm. Thus in the nucleus we have

$$\frac{\partial[I\kappa B\alpha]}{\partial t} = D_{I\kappa B\alpha} \nabla^2 [I\kappa B\alpha] - A_3 [I\kappa B\alpha][NF\kappa B] - d_{I\kappa B\alpha} [I\kappa B\alpha]. \quad (14)$$

Across the nuclear membrane, $I\kappa B\alpha$ diffuses and, given that it possesses a nuclear import sequence (Sachdev et al., 1998), we assume that it is actively transported (convected) towards the nucleus at velocity $\mathbf{a}_{I\kappa B\alpha}$ with constant magnitude or speed $a_{I\kappa B\alpha}$. Thus $I\kappa B\alpha$ in the nuclear membrane satisfies

$$\frac{\partial[I\kappa B\alpha]}{\partial t} = D_{I\kappa B\alpha} \nabla^2 [I\kappa B\alpha] + \nabla \cdot ([I\kappa B\alpha] \mathbf{a}_{I\kappa B\alpha}). \quad (15)$$

We suppose that A20 transcript diffuses at rate D_{A20t} and degrades at rate d_{A20t} in the cytoplasm, which yields

$$\frac{\partial[A20_t]}{\partial t} = D_{A20t} \nabla^2[A20_t] - d_{A20t}[A20_t]. \quad (16)$$

In the nucleus, we assume that A20 transcript diffuses and degrades at the same rates as in the cytoplasm. As with $I\kappa B\alpha$ transcript in Eq. (11) and in keeping with (Ashall et al., 2009) and the discussion in Section 2, we assume that A20 transcript production is a saturating function of NF- κ B, proportional (with constant of proportionality B_2) to a Hill function with Hill coefficient h and half-maximal rate M . Hence in the nucleus, we have

$$\frac{\partial[A20_t]}{\partial t} = D_{A20t} \nabla^2[A20_t] + B_2 \left(\frac{[NF\kappa B]^h}{[NF\kappa B]^h + M^h} \right) - d_{A20t}[A20_t]. \quad (17)$$

Across the nuclear membrane, A20 transcript diffuses

$$\frac{\partial[A20_t]}{\partial t} = D_{A20t} \nabla^2[A20_t]. \quad (18)$$

The protein A20 is present only in the cytoplasm in our model. It diffuses at rate D_{A20} and degrades at rate d_{A20} . It is also translated from A20 transcript at a rate E_2 , where we assume, as we did for $I\kappa B\alpha$ production in Eq. (13), that translation occurs at least some minimal distance H_2 from the nuclear membrane. Therefore we have

$$\frac{\partial[A20]}{\partial t} = D_{A20} \nabla^2[A20] + \theta_{r_2} E_2 [A20_t] - d_{A20}[A20], \quad (19)$$

where θ_{r_2} is defined after Eq. (13).

To complete our description of the model, we state initial and boundary conditions. As we mentioned at the end of the previous section, we suppose, as in Hoffmann et al. (2002) and Lipniacki et al. (2004), that the initial concentrations of all species are zero, except for $I\kappa B\alpha|NF\kappa B$ which equals a positive constant I_0 everywhere in the cytoplasm to reflect the fact that NF- κ B is held functionally inert in the cytoplasm by $I\kappa B\alpha$ until the cell is stimulated by an external signal. For ease of reference, we write our initial conditions as equations:

$$[X]_{t=0} = 0 \quad \text{where } [X] \text{ is any species except } [I\kappa B\alpha|NF\kappa B] \text{ in cytoplasm,} \quad (20)$$

$$[I\kappa B\alpha|NF\kappa B]_{t=0} = I_0 \quad \text{everywhere in cytoplasm.} \quad (21)$$

There are three boundaries in our model—the cell membrane, the outer nuclear membrane, and the inner nuclear membrane. For those species moving from one compartment to another across a boundary, we choose continuity of flux boundary conditions. Otherwise we choose zero flux boundary conditions. These conditions ensure that no molecules enter regions where they are not defined, that no molecules leave the cell, and that no molecules crossing a boundary are lost whilst doing so.

We can state our boundary conditions more explicitly. Let m denote a species moving across a boundary from compartment P to compartment Q by continuity of flux. Then we can let $[m_P]$ and $[m_Q]$ denote, respectively, the concentrations of m in P and Q , we can let D_m be the diffusion coefficient of m in P and Q , and at the boundary we can write

$$D_m \frac{\partial[m_P]}{\partial \mathbf{n}} = D_m \frac{\partial[m_Q]}{\partial \mathbf{n}} \quad \text{and} \quad [m_P] = [m_Q], \quad (22)$$

where \mathbf{n} is a unit normal.

Finally let $[m]$ denote the concentration of a species subject to zero flux at a boundary. Then at the boundary we can write

$$\frac{\partial[m]}{\partial \mathbf{n}} = 0, \quad (23)$$

where \mathbf{n} is again a unit normal.

4. Non-dimensionalisation

To find parameter values that yield oscillatory dynamics in our model, we follow the method used to find oscillatory dynamics in two similar recent spatio-temporal models of intracellular signalling (Terry et al., 2011; Sturrock et al., 2011). This method can be summarised as follows: non-dimensionalise the model, find non-dimensional parameter values that yield sustained oscillations, and then calculate dimensional parameters. The calculation of dimensional parameters involves fitting the experimentally observed oscillatory period and cell size to the non-dimensional oscillatory period and non-dimensional cell size.

We non-dimensionalise our model by first defining reference values. We define the reference concentrations

$$\begin{aligned} [IKKa]_{\text{ref}}, & \quad [IKKa|I\kappa B\alpha]_{\text{ref}}, & [IKKa|I\kappa B\alpha|NF\kappa B]_{\text{ref}}, \\ [I\kappa B\alpha|NF\kappa B]_{\text{ref}}, & [NF\kappa B]_{\text{ref}}, & [I\kappa B\alpha_t]_{\text{ref}}, \\ [I\kappa B\alpha]_{\text{ref}}, & [A20_t]_{\text{ref}}, & [A20]_{\text{ref}}, \end{aligned}$$

for, respectively,

$$\begin{aligned} [IKKa], & \quad [IKKa|I\kappa B\alpha], & [IKKa|I\kappa B\alpha|NF\kappa B], \\ [I\kappa B\alpha|NF\kappa B], & [NF\kappa B], & [I\kappa B\alpha_t], \\ [I\kappa B\alpha], & [A20_t], & [A20]. \end{aligned}$$

We also define the reference value τ for time t and the reference value L for the spatial variables x and y .

Next we define re-scaled variables. In the following, re-scaled variables have hats:

$$[\widehat{IKKa}] = \frac{[IKKa]}{[IKKa]_{\text{ref}}}, \quad [\widehat{IKKa|I\kappa B\alpha}] = \frac{[IKKa|I\kappa B\alpha]}{[IKKa|I\kappa B\alpha]_{\text{ref}}}, \quad (24)$$

$$[\widehat{IKKa|I\kappa B\alpha|NF\kappa B}] = \frac{[IKKa|I\kappa B\alpha|NF\kappa B]}{[IKKa|I\kappa B\alpha|NF\kappa B]_{\text{ref}}}, \quad (25)$$

$$[\widehat{I\kappa B\alpha|NF\kappa B}] = \frac{[I\kappa B\alpha|NF\kappa B]}{[I\kappa B\alpha|NF\kappa B]_{\text{ref}}}, \quad [\widehat{NF\kappa B}] = \frac{[NF\kappa B]}{[NF\kappa B]_{\text{ref}}}, \quad (26)$$

$$[\widehat{I\kappa B\alpha_t}] = \frac{[I\kappa B\alpha_t]}{[I\kappa B\alpha_t]_{\text{ref}}}, \quad [\widehat{I\kappa B\alpha}] = \frac{[I\kappa B\alpha]}{[I\kappa B\alpha]_{\text{ref}}}, \quad (27)$$

$$[\widehat{A20_t}] = \frac{[A20_t]}{[A20_t]_{\text{ref}}}, \quad [\widehat{A20}] = \frac{[A20]}{[A20]_{\text{ref}}}, \quad (28)$$

$$\hat{t} = \frac{t}{\tau}, \quad \hat{x} = \frac{x}{L}, \quad \hat{y} = \frac{y}{L}. \quad (29)$$

By substituting the scaling in (24)–(29) into our model (Eqs. (1)–(19)) and using the chain rule for differentiation, we obtain a non-dimensionalised model. In this non-dimensionalised model, the qualitative form of the equations is unchanged but the parameters and variables are all dimensionless. To be specific, we find in the cytoplasm that

$$\begin{aligned} \frac{\partial[\widehat{IKKa}]}{\partial \hat{t}} = & D_{IKKa}^* \nabla^2[\widehat{IKKa}] + \gamma_i^* \phi_{r_1}^* F^* - G^*[\widehat{IKKa}] \\ & - \gamma_i^* F^*[\widehat{IKKa}][\widehat{A20}] - A_{2,1}^*[\widehat{IKKa}][\widehat{I\kappa B\alpha}] \\ & - A_{2,1}^*[\widehat{IKKa}][\widehat{I\kappa B\alpha|NF\kappa B}] + C_{1,1}^*[\widehat{IKKa}][\widehat{I\kappa B\alpha}] \\ & + C_{2,1}^*[\widehat{IKKa|I\kappa B\alpha|NF\kappa B}] - d_{IKKa}^*[\widehat{IKKa}], \end{aligned} \quad (30)$$

$$\frac{\partial[\widehat{\text{IKKa}}|\widehat{\text{IkB}\alpha}]}{\partial\hat{t}} = D_{\widehat{\text{IKKa}}|\widehat{\text{IkB}\alpha}}^* \nabla^2[\widehat{\text{IKKa}}|\widehat{\text{IkB}\alpha}] + A_{1,2}^*[\widehat{\text{IKKa}}][\widehat{\text{IkB}\alpha}] - C_{1,2}^*[\widehat{\text{IKKa}}|\widehat{\text{IkB}\alpha}], \quad (31)$$

$$\frac{\partial[\widehat{\text{IKKa}}|\widehat{\text{IkB}\alpha}|\widehat{\text{NF}\kappa\text{B}}]}{\partial\hat{t}} = D_{\widehat{\text{IKKa}}|\widehat{\text{IkB}\alpha}|\widehat{\text{NF}\kappa\text{B}}}^* \nabla^2[\widehat{\text{IKKa}}|\widehat{\text{IkB}\alpha}|\widehat{\text{NF}\kappa\text{B}}] + A_{2,2}^*[\widehat{\text{IKKa}}][\widehat{\text{IkB}\alpha}|\widehat{\text{NF}\kappa\text{B}}] - C_{2,2}^*[\widehat{\text{IKKa}}|\widehat{\text{IkB}\alpha}|\widehat{\text{NF}\kappa\text{B}}], \quad (32)$$

$$\frac{\partial[\widehat{\text{IkB}\alpha}|\widehat{\text{NF}\kappa\text{B}}]}{\partial\hat{t}} = D_{\widehat{\text{IkB}\alpha}|\widehat{\text{NF}\kappa\text{B}}}^* \nabla^2[\widehat{\text{IkB}\alpha}|\widehat{\text{NF}\kappa\text{B}}] + A_{3,1}^*[\widehat{\text{IkB}\alpha}][\widehat{\text{NF}\kappa\text{B}}] - A_{2,3}^*[\widehat{\text{IKKa}}][\widehat{\text{IkB}\alpha}|\widehat{\text{NF}\kappa\text{B}}] - K_1^*[\widehat{\text{IkB}\alpha}|\widehat{\text{NF}\kappa\text{B}}], \quad (33)$$

$$\frac{\partial[\widehat{\text{NF}\kappa\text{B}}]}{\partial\hat{t}} = D_{\widehat{\text{NF}\kappa\text{B}}}^* \nabla^2[\widehat{\text{NF}\kappa\text{B}}] - A_{3,2}^*[\widehat{\text{IkB}\alpha}][\widehat{\text{NF}\kappa\text{B}}] + C_{2,3}^*[\widehat{\text{IKKa}}|\widehat{\text{IkB}\alpha}|\widehat{\text{NF}\kappa\text{B}}] + K_2^*[\widehat{\text{IkB}\alpha}|\widehat{\text{NF}\kappa\text{B}}], \quad (34)$$

$$\frac{\partial[\widehat{\text{IkB}\alpha}_t]}{\partial\hat{t}} = D_{\widehat{\text{IkB}\alpha}_t}^* \nabla^2[\widehat{\text{IkB}\alpha}_t] - d_{\widehat{\text{IkB}\alpha}_t}^*[\widehat{\text{IkB}\alpha}_t], \quad (35)$$

$$\frac{\partial[\widehat{\text{IkB}\alpha}]}{\partial\hat{t}} = D_{\widehat{\text{IkB}\alpha}}^* \nabla^2[\widehat{\text{IkB}\alpha}] + \theta_{i_2}^* E_1^*[\widehat{\text{IkB}\alpha}_t] - A_{1,3}^*[\widehat{\text{IKKa}}][\widehat{\text{IkB}\alpha}] - A_{3,3}^*[\widehat{\text{IkB}\alpha}][\widehat{\text{NF}\kappa\text{B}}] - d_{\widehat{\text{IkB}\alpha}}^*[\widehat{\text{IkB}\alpha}], \quad (36)$$

$$\frac{\partial[\widehat{\text{A20}}_t]}{\partial\hat{t}} = D_{\widehat{\text{A20}}_t}^* \nabla^2[\widehat{\text{A20}}_t] - d_{\widehat{\text{A20}}_t}^*[\widehat{\text{A20}}_t], \quad (37)$$

$$\frac{\partial[\widehat{\text{A20}}]}{\partial\hat{t}} = D_{\widehat{\text{A20}}}^* \nabla^2[\widehat{\text{A20}}] + \theta_{i_2}^* E_2^*[\widehat{\text{A20}}_t] - d_{\widehat{\text{A20}}}^*[\widehat{\text{A20}}], \quad (38)$$

and in the nuclear membrane we find that

$$\frac{\partial[\widehat{\text{IkB}\alpha}|\widehat{\text{NF}\kappa\text{B}}]}{\partial\hat{t}} = D_{\widehat{\text{IkB}\alpha}|\widehat{\text{NF}\kappa\text{B}}}^* \nabla^2[\widehat{\text{IkB}\alpha}|\widehat{\text{NF}\kappa\text{B}}] - \nabla \cdot ([\widehat{\text{IkB}\alpha}|\widehat{\text{NF}\kappa\text{B}}] \mathbf{a}_{\widehat{\text{IkB}\alpha}|\widehat{\text{NF}\kappa\text{B}}}^*), \quad (39)$$

$$\frac{\partial[\widehat{\text{NF}\kappa\text{B}}]}{\partial\hat{t}} = D_{\widehat{\text{NF}\kappa\text{B}}}^* \nabla^2[\widehat{\text{NF}\kappa\text{B}}] + \nabla \cdot ([\widehat{\text{NF}\kappa\text{B}}] \mathbf{a}_{\widehat{\text{NF}\kappa\text{B}}}^*), \quad (40)$$

$$\frac{\partial[\widehat{\text{IkB}\alpha}_t]}{\partial\hat{t}} = D_{\widehat{\text{IkB}\alpha}_t}^* \nabla^2[\widehat{\text{IkB}\alpha}_t], \quad (41)$$

$$\frac{\partial[\widehat{\text{IkB}\alpha}]}{\partial\hat{t}} = D_{\widehat{\text{IkB}\alpha}}^* \nabla^2[\widehat{\text{IkB}\alpha}] + \nabla \cdot ([\widehat{\text{IkB}\alpha}] \mathbf{a}_{\widehat{\text{IkB}\alpha}}^*), \quad (42)$$

$$\frac{\partial[\widehat{\text{A20}}_t]}{\partial\hat{t}} = D_{\widehat{\text{A20}}_t}^* \nabla^2[\widehat{\text{A20}}_t], \quad (43)$$

and in the nucleus we find that

$$\frac{\partial[\widehat{\text{IkB}\alpha}|\widehat{\text{NF}\kappa\text{B}}]}{\partial\hat{t}} = D_{\widehat{\text{IkB}\alpha}|\widehat{\text{NF}\kappa\text{B}}}^* \nabla^2[\widehat{\text{IkB}\alpha}|\widehat{\text{NF}\kappa\text{B}}] + A_{3,1}^*[\widehat{\text{IkB}\alpha}][\widehat{\text{NF}\kappa\text{B}}], \quad (44)$$

$$\frac{\partial[\widehat{\text{NF}\kappa\text{B}}]}{\partial\hat{t}} = D_{\widehat{\text{NF}\kappa\text{B}}}^* \nabla^2[\widehat{\text{NF}\kappa\text{B}}] - A_{3,2}^*[\widehat{\text{IkB}\alpha}][\widehat{\text{NF}\kappa\text{B}}], \quad (45)$$

$$\frac{\partial[\widehat{\text{IkB}\alpha}_t]}{\partial\hat{t}} = D_{\widehat{\text{IkB}\alpha}_t}^* \nabla^2[\widehat{\text{IkB}\alpha}_t] + B_1^* \left(\frac{[\widehat{\text{NF}\kappa\text{B}}]^h}{([\widehat{\text{NF}\kappa\text{B}}]^h + (M^*)^h)} \right) - d_{\widehat{\text{IkB}\alpha}_t}^*[\widehat{\text{IkB}\alpha}_t], \quad (46)$$

$$\frac{\partial[\widehat{\text{IkB}\alpha}]}{\partial\hat{t}} = D_{\widehat{\text{IkB}\alpha}}^* \nabla^2[\widehat{\text{IkB}\alpha}] - A_{3,3}^*[\widehat{\text{IkB}\alpha}][\widehat{\text{NF}\kappa\text{B}}] - d_{\widehat{\text{IkB}\alpha}}^*[\widehat{\text{IkB}\alpha}], \quad (47)$$

$$\frac{\partial[\widehat{\text{A20}}_t]}{\partial\hat{t}} = D_{\widehat{\text{A20}}_t}^* \nabla^2[\widehat{\text{A20}}_t] + B_2^* \left(\frac{[\widehat{\text{NF}\kappa\text{B}}]^h}{([\widehat{\text{NF}\kappa\text{B}}]^h + (M^*)^h)} \right) - d_{\widehat{\text{A20}}_t}^*[\widehat{\text{A20}}_t], \quad (48)$$

where the ∇ operator is now with respect to the non-dimensional spatial variables \hat{x} and \hat{y} , where the directions of the active transport vectors are unchanged but now have magnitudes $a_{\widehat{\text{NF}\kappa\text{B}}}^*$, $a_{\widehat{\text{IkB}\alpha}}^*$, and $a_{\widehat{\text{IkB}\alpha}|\widehat{\text{NF}\kappa\text{B}}}^*$ for the species $\widehat{\text{NF}\kappa\text{B}}$, $\widehat{\text{IkB}\alpha}$, and $\widehat{\text{IkB}\alpha}|\widehat{\text{NF}\kappa\text{B}}$ respectively, and where non-dimensional parameters are related to dimensional ones as follows. For diffusion coefficients, degradation rates, and active transport rates, we have

$$D_X^* = \frac{D_X \tau}{L^2}, \quad d_Y^* = d_Y \tau, \quad a_Z^* = \frac{a_Z \tau}{L}, \quad (49)$$

for X representing any of the species in the model, Y representing IKKa, IkB α transcript, IkB α , A20 transcript, and A20, and Z representing IkB α |NF κ B, NF κ B, and IkB α .

The term γ_t^* is a function of the non-dimensional time variable \hat{t} such that $\gamma_t^* = 0$ if $\hat{t} < T^*$ and $\gamma_t^* = 1$ otherwise, where

$$T^* = \frac{T}{\tau}. \quad (50)$$

Similarly the term $\phi_{r_1}^*$ is a function of the non-dimensional spatial variables \hat{x} and \hat{y} , defined over points (\hat{x}, \hat{y}) in the cytoplasm such that $\phi_{r_1}^* = 1$ if the distance \hat{r}_1 of the point (\hat{x}, \hat{y}) from the cell membrane is less than or equal to H_1^* non-dimensional spatial units and $\phi_{r_1}^* = 0$ otherwise, where

$$H_1^* = \frac{H_1}{L}, \quad (51)$$

and the term $\theta_{i_2}^*$ is also a function of \hat{x} and \hat{y} , defined over points (\hat{x}, \hat{y}) in the cytoplasm such that $\theta_{i_2}^* = 0$ if the distance \hat{r}_2 of the point (\hat{x}, \hat{y}) from the nuclear membrane is less than H_2^* non-dimensional spatial units and $\theta_{i_2}^* = 1$ otherwise, where

$$H_2^* = \frac{H_2}{L}. \quad (52)$$

The remaining parameter relationships are

$$A_{1,1}^* = A_1[\widehat{\text{IkB}\alpha}]_{\text{ref}} \tau, \quad A_{1,2}^* = \frac{A_1[\widehat{\text{IKKa}}]_{\text{ref}}[\widehat{\text{IkB}\alpha}]_{\text{ref}} \tau}{[\widehat{\text{IKKa}}|\widehat{\text{IkB}\alpha}]_{\text{ref}}}, \quad (53)$$

$$A_{1,3}^* = A_1[\widehat{\text{IKKa}}]_{\text{ref}} \tau, \quad A_{2,1}^* = A_2[\widehat{\text{IkB}\alpha}|\widehat{\text{NF}\kappa\text{B}}]_{\text{ref}} \tau, \quad (54)$$

$$A_{2,2}^* = \frac{A_2[\widehat{\text{IKKa}}]_{\text{ref}}[\widehat{\text{IkB}\alpha}|\widehat{\text{NF}\kappa\text{B}}]_{\text{ref}} \tau}{[\widehat{\text{IKKa}}|\widehat{\text{IkB}\alpha}|\widehat{\text{NF}\kappa\text{B}}]_{\text{ref}}}, \quad (55)$$

$$A_{2,3}^* = A_2[\widehat{\text{IKKa}}]_{\text{ref}} \tau, \quad A_{3,1}^* = \frac{A_3[\widehat{\text{IkB}\alpha}]_{\text{ref}}[\widehat{\text{NF}\kappa\text{B}}]_{\text{ref}} \tau}{[\widehat{\text{IkB}\alpha}|\widehat{\text{NF}\kappa\text{B}}]_{\text{ref}}}, \quad (56)$$

$$A_{3,2}^* = A_3[\widehat{\text{IkB}\alpha}]_{\text{ref}} \tau, \quad A_{3,3}^* = A_3[\widehat{\text{NF}\kappa\text{B}}]_{\text{ref}} \tau, \quad (57)$$

$$B_1^* = \frac{B_1 \tau}{[\widehat{\text{IkB}\alpha}_t]_{\text{ref}}}, \quad B_2^* = \frac{B_2 \tau}{[\widehat{\text{A20}}_t]_{\text{ref}}}, \quad (58)$$

$$C_{1,1}^* = \frac{C_1[\widehat{\text{IKKa}}|\widehat{\text{IkB}\alpha}]_{\text{ref}} \tau}{[\widehat{\text{IKKa}}]_{\text{ref}}}, \quad C_{1,2}^* = C_1 \tau, \quad (59)$$

$$C_{2,1}^* = \frac{C_2[\widehat{\text{IKKa}}|\widehat{\text{IkB}\alpha}|\widehat{\text{NF}\kappa\text{B}}]_{\text{ref}} \tau}{[\widehat{\text{IKKa}}]_{\text{ref}}}, \quad C_{2,2}^* = C_2 \tau, \quad (60)$$

$$C_{2,3}^* = \frac{C_2[\widehat{\text{IKKa}}|\widehat{\text{IkB}\alpha}|\widehat{\text{NF}\kappa\text{B}}]_{\text{ref}} \tau}{[\widehat{\text{NF}\kappa\text{B}}]_{\text{ref}}}, \quad (61)$$

$$E_1^* = \frac{E_1[\widehat{\text{IkB}\alpha}_t]_{\text{ref}} \tau}{[\widehat{\text{IkB}\alpha}]_{\text{ref}}}, \quad E_2^* = \frac{E_2[\widehat{\text{A20}}_t]_{\text{ref}} \tau}{[\widehat{\text{A20}}]_{\text{ref}}}, \quad (62)$$

$$F^* = \frac{F \tau}{[\widehat{\text{IKKa}}]_{\text{ref}}}, \quad G^* = G \tau, \quad J^* = J[\widehat{\text{A20}}]_{\text{ref}} \tau, \quad (63)$$

$$K_1^* = K\tau, \quad K_2^* = \frac{K[\text{IkB}\alpha|\text{NF}\kappa\text{B}]_{\text{ref}}\tau}{[\text{NF}\kappa\text{B}]_{\text{ref}}}, \quad M^* = \frac{M}{[\text{NF}\kappa\text{B}]_{\text{ref}}}. \quad (64)$$

Combining the scaling in (24)–(29) with the initial conditions in the dimensional model (Eqs. (20) and (21)) gives us initial conditions for the non-dimensionalised model:

$$[\widehat{X}]_{\tilde{t}=0} = 0 \text{ where } [\widehat{X}] \text{ is any species except } [\text{IkB}\alpha|\widehat{\text{NF}\kappa\text{B}}] \text{ in cytoplasm,} \quad (65)$$

$$[\text{IkB}\alpha|\widehat{\text{NF}\kappa\text{B}}]_{\tilde{t}=0} = I_0^* = \frac{I_0}{[\text{IkB}\alpha|\text{NF}\kappa\text{B}]_{\text{ref}}} \text{ in cytoplasm.} \quad (66)$$

Similarly, we can combine the scaling in (24)–(29) with the boundary conditions in the dimensional model (Eqs. (22) and (23)) to obtain boundary conditions in the non-dimensionalised model. Trivially we find that the conditions stated in Eqs. (22) and (23) still hold, except that D_m , $[m_p]$, $[m_Q]$, and $[m]$ are replaced in these equations by D_m^* , $[\hat{m}_p]$, $[\hat{m}_Q]$, and $[\hat{m}]$, respectively.

5. Simulations

We can numerically solve our non-dimensionalised model (Eqs. (30)–(48)) using the COMSOL/FEMLAB package, which uses the finite element technique. In using this package to perform simulations, we choose triangular basis elements and Lagrange quadratic basis functions along with a backward Euler time-stepping method of integration.

Before conducting simulations we must define a geometry on which to conduct them and choose values for the model parameters. Our goal is to make choices that yield oscillatory dynamics. We can allow our decisions to be influenced by two recent studies of intracellular pathways which adopt the same PDE approach used in our model (Terry et al., 2011; Sturrock et al., 2011). We define a geometry with similar non-dimensional size as in these studies. Also as in these studies, we reduce the number of parameters in our model by making simplifying assumptions: for instance, all natural degradation rates are set equal and all species are assumed to have the same diffusion rate. Simplifying assumptions of this kind are often made in models with a large number of unknown parameters, including previous models of the NF- κ B pathway (Nelson et al., 2004; Hoffmann et al., 2002; Lipniacki et al., 2004). A simplified approach is sensible here because our purpose is an initial spatio-temporal study. In future work, we will take into account the fact that the diffusion coefficient of a molecule depends on its size—a larger molecule has a smaller diffusion coefficient.

To find parameter values, we begin by considering values with the same order of magnitude as corresponding non-dimensional parameters in Terry et al. (2011) and Sturrock et al. (2011) where corresponding parameters exist; examples of such parameters are diffusion and natural degradation rates. Using all these choices and assumptions places us in a position to begin a simulation study. From this position, we have carried out a systematic study that led us to parameter values yielding oscillatory dynamics. We fine tuned our parameter values by bearing in mind values used in previous studies (Nelson et al., 2004; Lipniacki et al., 2004; Ashall et al., 2009), and also by bearing in mind experimental and theoretical results suggesting, for instance, that a significant proportion of NF- κ B is freed from IkB α |NF κ B by signalling (Nelson et al., 2004; Lipniacki et al., 2004) and that IKKa concentration peaks quickly after the onset of continuous cell stimulation and then rapidly decreases (Lee et al., 2000; Lipniacki et al., 2004).

The geometry on which we define our non-dimensionalised model is:

- a circle representing the nucleus, radius 0.5, centre (0,0),
- an annular region, representing the nuclear membrane, bounded by the following circles: radius 0.5, centre (0,0); radius 0.52, centre (0,0),
- an annular region, representing the cytoplasm, bounded by the following circles: radius 0.52, centre (0,0); radius 1.2, centre (0,0).

We depict this geometry in Fig. 3. It was necessary to suppose the nucleus was centred at (0,0) in view of our active transport assumptions (see paragraph containing Eq. (6)). Although we initially performed simulations on a circular cell, we later found that oscillations are somewhat robust to changes in the shape of the cell and its nucleus, as well as the ratio of nuclear to cytoplasmic size (discussed below in Section 5.2).

Next we explicitly state the simplifying assumptions that we made for the parameters. We assume that all diffusion coefficients are equal to a positive constant D^* , all natural degradation rates are equal to a positive constant d^* , and all active transport rates are equal to a positive constant a^* . In other words, we have

$$D_X^* = D^*, \quad d_Y^* = d^*, \quad a_Z^* = a^*, \quad (67)$$

for X representing any of the species in the model, Y representing IKKa, IkB α transcript, IkB α , A20 transcript, and A20, and Z representing IkB α |NF κ B, NF- κ B, and IkB α .

To allow the resting cell to reach an equilibrium state, we do not allow cell stimulation to begin until time $\tilde{t} = T^*$, where

$$T^* = 300. \quad (68)$$

We then find oscillatory dynamics (with period 120 non-dimensional time units, simulating up to $\tilde{t} = 1400$) for the following parameter choices:

$$D^* = 0.01, \quad d^* = 0.05, \quad a^* = 1.5, \quad (69)$$

$$A_{1,1}^* = A_{1,2}^* = A_{1,3}^* = A_{3,1}^* = A_{3,2}^* = A_{3,3}^* = C_{1,1}^* = C_{1,2}^* = E_1^* = E_2^* = 1.5, \quad (70)$$

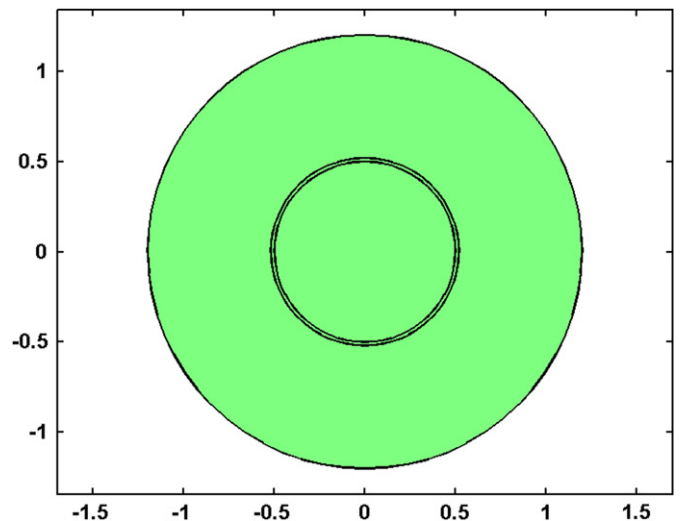


Fig. 3. The non-dimensionalised model (Eqs. (30)–(48)) holds on the green geometry shown here. The geometry is a cell with three compartments—the nucleus (the area within the inner circle), the nuclear membrane (the thin annulus between the two inner circles), and the cytoplasm (the annulus between the two outer circles). (For interpretation of the references to colour in this figure legend, the reader is referred to the web version of this article.)

$$A_{2,1}^* = A_{2,2}^* = A_{2,3}^* = C_{2,1}^* = C_{2,2}^* = C_{2,3}^* = 3, \quad (71)$$

$$B_1^* = B_2^* = 0.02, \quad F^* = 0.2, \quad G^* = 0.15, \quad H_1^* = H_2^* = 0.2, \quad (72)$$

$$J^* = 5, \quad K_1^* = K_2^* = 0.0001, \quad M^* = 0.065, \quad h = 2, \quad (73)$$

$$I_0^* = 1 \quad (\text{initial condition}). \quad (74)$$

Figs. 4–9 show simulation results of the non-dimensionalised model, performed on the geometry depicted in Fig. 3, with the parameter choices in Eqs. (67)–(74). We discuss these figures in Section 5.1 below. In the remainder of the current section, we use our non-dimensional parameter choices to calculate dimensional parameter values that generate sustained oscillations. To do this, we first estimate the reference time τ and reference length L . As indicated at the start of Section 4, the reference time τ is chosen to make the oscillatory period in the dimensional model equal the experimentally observed oscillatory period. Now we have said that the oscillatory period in our simulations is 120 non-dimensional time units. But by (29), we have $t = \hat{t}\tau$, so 1 non-dimensional time unit is τ dimensional time units. Hence the oscillatory period in the dimensional model is 120τ dimensional time units. We set the oscillatory period in the dimensional model equal to

the experimentally observed oscillatory period, which is 100 min or 6000 s (Nelson et al., 2004), to obtain $120\tau = 6000$ s, so that $\tau = 50.0$ s. (75)

Note that we shall state all dimensional parameters to three significant figures.

Using (50), (68), and (75), we find the time T at which cell stimulation begins in the dimensional model:

$$T = T^*\tau = 250 \text{ min}. \quad (76)$$

In all plots below, time is displayed in dimensional units and shifted so that continuous cell stimulation begins at 100 min.

As indicated at the start of Section 4, the reference length L is chosen to make the cell in the dimensional model the same size as a real-world cell. The diameter of our non-dimensional cell is 2.4 non-dimensionalised spatial units (Fig. 3) or $2.4L$ dimensional spatial units (using (29)). Also, the diameter of cells used in experiments of the continuous stimulation of the NF- κ B pathway is around 30 μm to 40 μm (Nelson et al., 2004; Ashall et al., 2009), so we set $2.4L = 35 \mu\text{m}$, which yields

$$L = 14.6 \mu\text{m}. \quad (77)$$

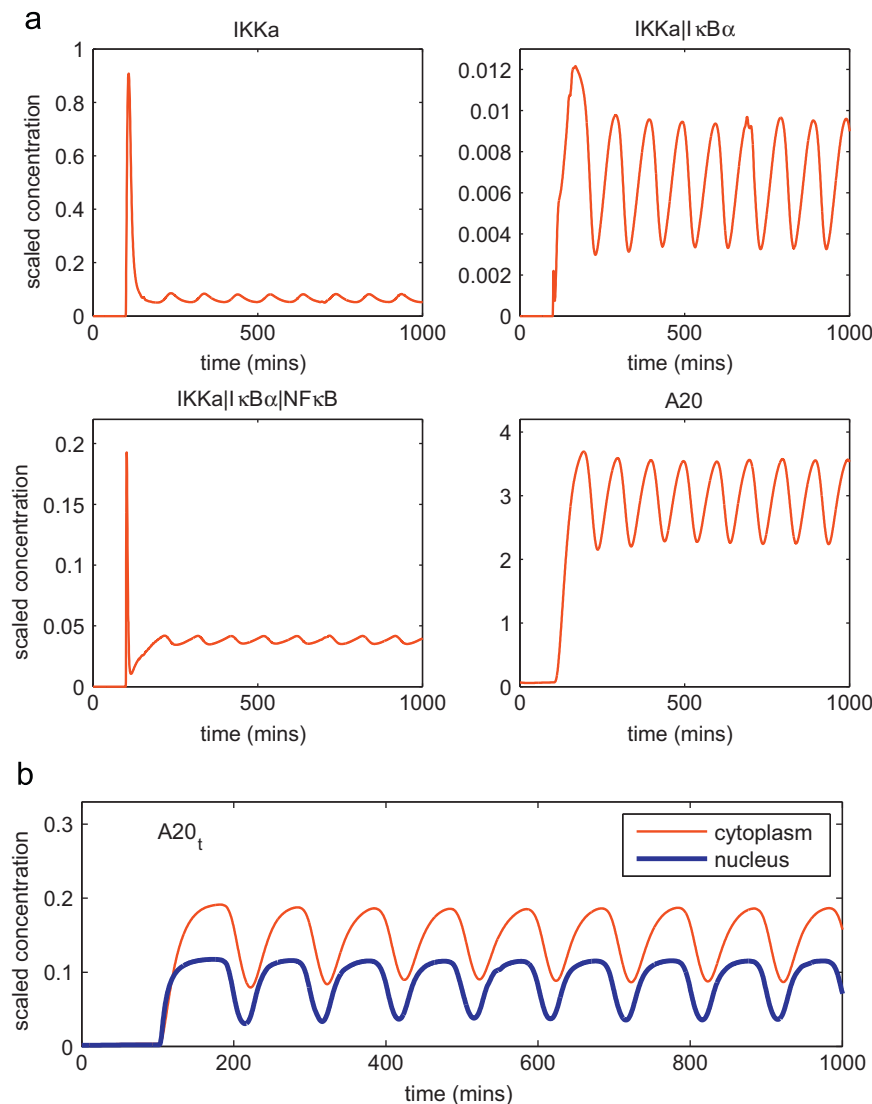


Fig. 4. Plots showing the total concentration over time for (a) the cytoplasmic species IKKa, IKKa|κBα, IKKa|κBα|NFκB, and A20, and (b) the species A20 transcript, created from a simulation of the non-dimensionalised model (Eqs. (30)–(48)) with geometry as in Fig. 3 and parameters determined by (67)–(74). Time is displayed here and in subsequent figures to correspond to continuous cell stimulation from 100 min onwards. Concentrations are shown in non-dimensional units.

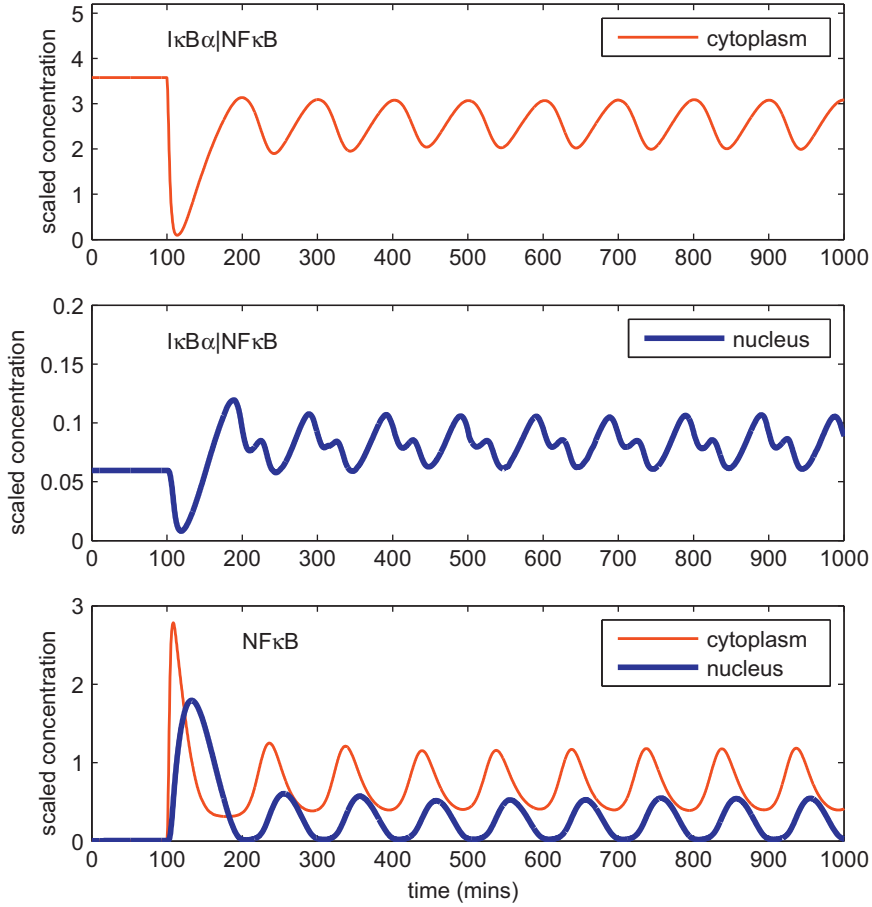


Fig. 5. Plots showing the total concentration over time for the species $I\kappa B\alpha|NF\kappa B$ and $NF\kappa B$, created from a simulation of the non-dimensionalised model (Eqs. (30)–(48)) with geometry as in Fig. 3 and parameters determined by (67)–(74). Continuous cell stimulation begins at 100 min. Concentrations are shown in non-dimensional units.

Using (51), (72), and (77), we find the maximum distance H_1 of IKK activation from the cell membrane:

$$H_1 = H_1^* L = 2.92 \mu\text{m}. \quad (78)$$

Similarly, by (52), (72), and (77), we find the minimum distance H_2 of translation from the nuclear membrane:

$$H_2 = H_2^* L = 2.92 \mu\text{m}. \quad (79)$$

Using (49), (67), (69), (75), and (77), we find diffusion, natural degradation, and active transport rates:

$$D_X = \frac{D^* L^2}{\tau} = 0.0425 \mu\text{m}^2 \text{s}^{-1}, \quad (80)$$

$$d_Y = \frac{d^*}{\tau} = 0.00100 \text{s}^{-1}, \quad (81)$$

$$a_Z = \frac{a^* L}{\tau} = 0.438 \mu\text{m} \text{s}^{-1}, \quad (82)$$

for X representing any of the species in the model, Y representing IKKa, $I\kappa B\alpha$ transcript, $I\kappa B\alpha$, A20 transcript, and A20, and Z representing $I\kappa B\alpha|NF\kappa B$, $NF\kappa B$, and $I\kappa B\alpha$.

Our value for the diffusion coefficients of $0.0425 \mu\text{m}^2 \text{s}^{-1}$ is approximately an order of magnitude larger than the diffusion coefficients in the two similar recent spatio-temporal studies of intracellular signalling mentioned earlier in this section (Terry et al., 2011; Sturrock et al., 2011). But how does our value compare to experimentally measured diffusion coefficients? Brown and Kholodenko state that the diffusion coefficient of soluble proteins in the cytoplasm has been estimated by various

means to be from $10^{-8} \text{cm}^2 \text{s}^{-1}$ to $10^{-7} \text{cm}^2 \text{s}^{-1}$, that is, from $1 \mu\text{m}^2 \text{s}^{-1}$ to $10 \mu\text{m}^2 \text{s}^{-1}$, though they note that it can be considerably lower if the protein reversibly binds to immobile components of the cell (Brown and Kholodenko, 1999). Our diffusion coefficient estimate implicitly includes reversible binding to genes (for $NF\kappa B$) or ribosomes (for $I\kappa B\alpha$ transcript and A20 transcript) and interaction with nuclear pore complexes (for $I\kappa B\alpha|NF\kappa B$, $NF\kappa B$, $I\kappa B\alpha$ transcript, $I\kappa B\alpha$, A20 transcript, and A20). It seems reasonable to expect genes and nuclear pore complexes to be rather less mobile than freely diffusing proteins and transcript molecules. Ribosomes may be free in the cytoplasm or bound to the endoplasmic reticulum; in either case the diffusion of a transcript molecule will be slowed by reversible binding to a ribosome. Hence our estimate is not necessarily inconsistent with experimental measurements. When we include greater spatial structure in our model in future work, we may find that sustained oscillations require a larger diffusion coefficient than our current estimate. For the moment, we have found that sustained oscillations may occur in our model for a range of values for the diffusion coefficient that spans one order of magnitude (see Eq. (100) below). We have also plotted the behaviour in cytoplasmic and nuclear $NF\kappa B$ for various values of the diffusion coefficient in Fig. 11 below.

We offer a further comment on experimental measurements of diffusion. Klonis et al. (2002) point out that diffusion rates of macromolecules in the cytoplasm and nucleus are up to 100 times slower than in aqueous buffers, whilst Matsuda et al. (2008) give measurements in aqueous buffers of around $10^{-7} \text{cm}^2 \text{s}^{-1}$ or $10 \mu\text{m}^2 \text{s}^{-1}$. Reducing the measurement of Matsuda et al. by a

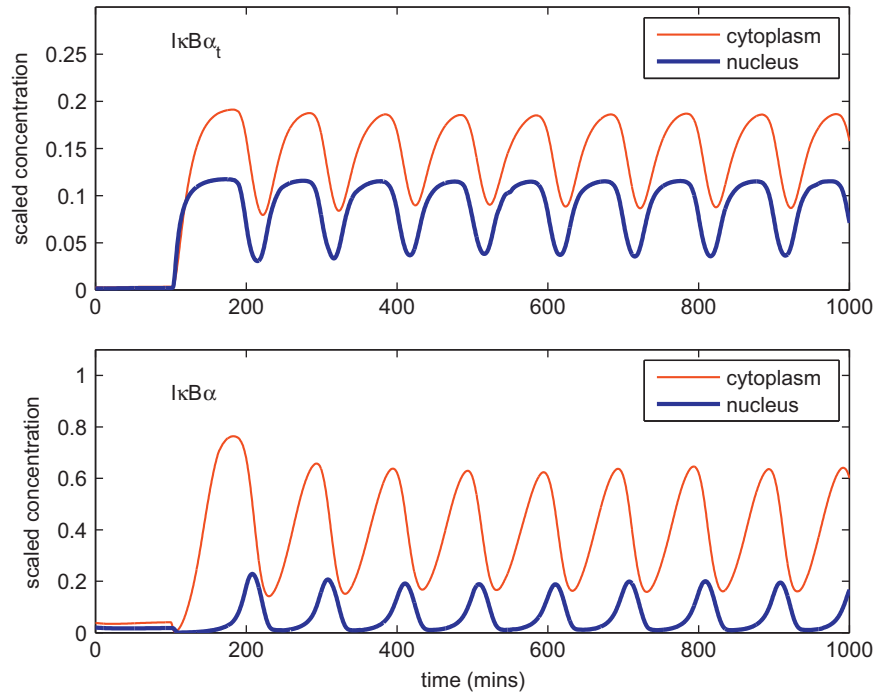


Fig. 6. Plots showing the total concentration over time for the species $I\kappa B\alpha$ transcript (shown as $I\kappa B\alpha_t$) and $I\kappa B\alpha$, created from a simulation of the non-dimensionalised model (Eqs. (30)–(48)) with geometry as in Fig. 3 and parameters determined by (67)–(74). Continuous cell stimulation begins at 100 min. Concentrations are shown in non-dimensional units.

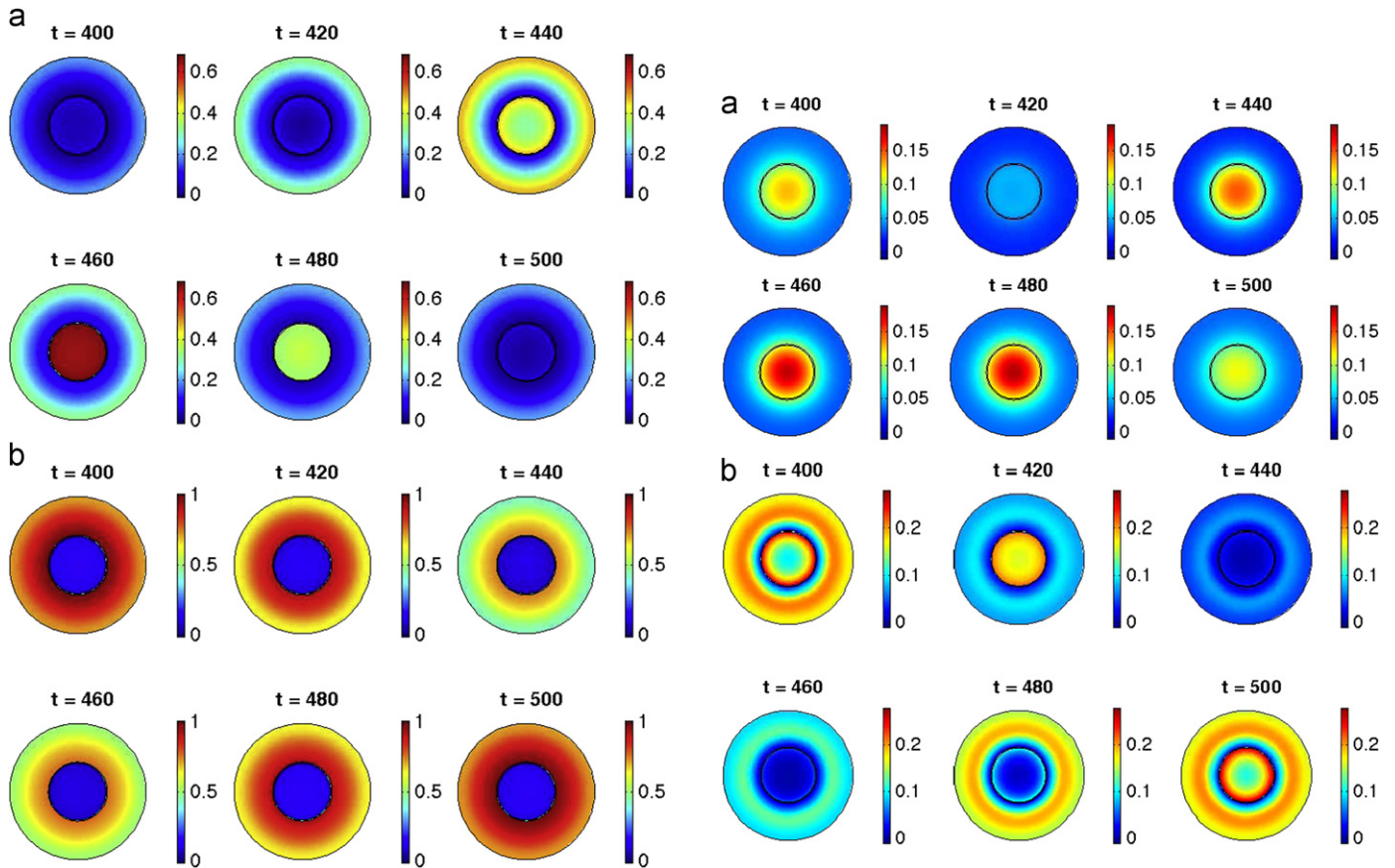


Fig. 7. Plots showing the spatial distribution of (a) NF- κ B and (b) $I\kappa B\alpha$ /NF κ B concentrations at 20 min intervals over a typical period, from 400 to 500 min, where continuous cell stimulation begins at 100 min. Plots created from a simulation of the non-dimensionalised model (Eqs. (30)–(48)) with geometry as in Fig. 3 and parameters determined by (67)–(74). Concentrations are shown in non-dimensional units.

Fig. 8. Plots showing the spatial distribution of (a) $I\kappa B\alpha$ transcript and (b) $I\kappa B\alpha$ concentrations at 20 min intervals over a typical period, from 400 to 500 min, where continuous cell stimulation begins at 100 min. Plots created from a simulation of the non-dimensionalised model (Eqs. (30)–(48)) with geometry as in Fig. 3 and parameters determined by (67)–(74). Concentrations are shown in non-dimensional units.

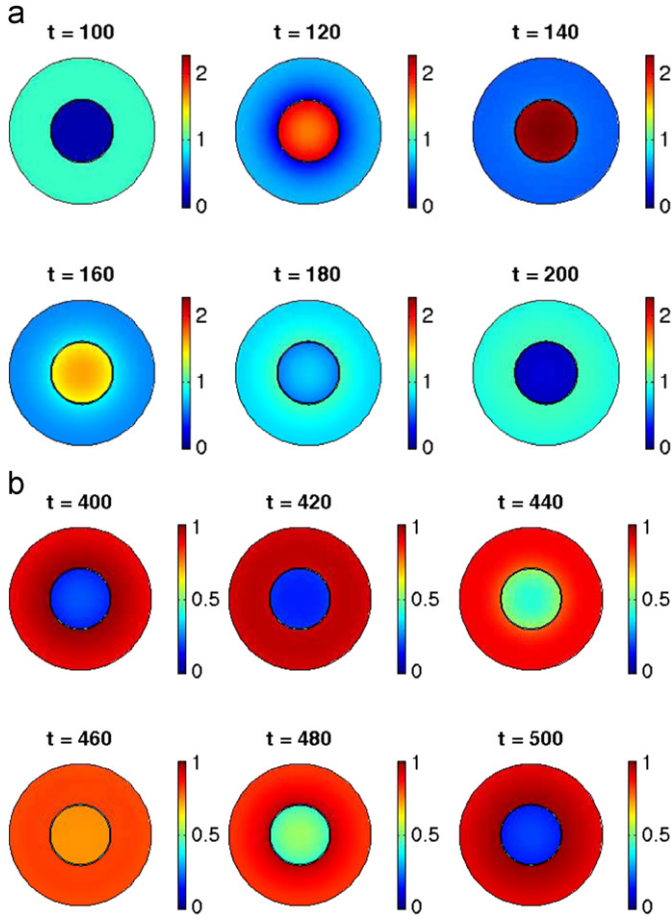


Fig. 9. Plots showing the spatial distribution of $IKK\alpha|NF\kappa B+NF-\kappa B$ concentration over (a) the first 100 min of cell stimulation and (b) a typical period, from 400 to 500 min. Continuous cell stimulation begins at 100 min. Plots created from a simulation of the non-dimensionalised model (Eqs. (30)–(48)) with geometry as in Fig. 3 and parameters determined by (67)–(74). Concentrations are shown in non-dimensional units. Notice the similarity of the behaviour shown here with the behaviour of the NF- κ B-containing species in the experimental images of Fig. 1.

factor of 100 gives $0.1 \mu\text{m}^2 \text{s}^{-1}$, which is about twice as big as our diffusion coefficient estimate, a difference that is plausible given our comments above on how we have not explicitly modelled reversible binding processes.

The natural degradation rate 0.00100 s^{-1} in (81) is similar to recently fitted but experimentally constrained values of 0.0003 s^{-1} and 0.0005 s^{-1} for $IKK\alpha$ transcript and $IKK\alpha$ respectively (Ashall et al., 2009). It is also similar to the fitted values of 0.0005 s^{-1} , 0.00048 s^{-1} , and 0.00143 s^{-1} for, respectively, $IKK\alpha$, A20 transcript, and A20 degradation in Ashall et al. (2009).

Ribbeck and Gorlich estimate that translocating material can cross the central channel of nuclear pore complexes (NPCs) at speeds of at least $0.5 \mu\text{m} \text{ s}^{-1}$ (Ribbeck and Gorlich, 2001). However, not all of the nuclear membrane consists of the central channels of NPCs. Hence this estimate is quite consistent with our active transport rate across the nuclear membrane of $0.438 \mu\text{m} \text{ s}^{-1}$ in (82) because our model makes the simplifying assumption that convective transport takes place throughout the entire region of the nuclear membrane.

From (59), (70), and (75), we find the dissociation rate C_1 of $IKK\alpha|IKK\alpha$ due to catalytic activity of $IKK\alpha$:

$$C_1 = \frac{C_{1,2}^*}{\tau} = 0.0300 \text{ s}^{-1}. \quad (83)$$

From (60), (71), and (75), we find the dissociation rate C_2 of $IKK\alpha|IKK\alpha|NF\kappa B$ due to catalytic activity of $IKK\alpha$:

$$C_2 = \frac{C_{2,2}^*}{\tau} = 0.0600 \text{ s}^{-1}. \quad (84)$$

From (63), (72), and (75), we find the rate G of spontaneous deactivation of $IKK\alpha$:

$$G = \frac{G^*}{\tau} = 0.003 \text{ s}^{-1}. \quad (85)$$

Our values for C_1 , C_2 , and G are of the same order of magnitude as analogous parameters in other models (Lipniacki et al., 2004; Nelson et al., 2004; Hoffmann et al., 2002).

From (64), (73), and (75), we find the dissociation rate K of $IKK\alpha|NF\kappa B$ due to the natural degradation of the $IKK\alpha$ in it:

$$K = \frac{K_1^*}{\tau} = 0.00000600 \text{ s}^{-1}. \quad (86)$$

This value is close to the experimentally measured rate for K of 0.00002 s^{-1} (Pando and Verma, 2000).

From (73), we see that the Hill coefficient h for our NF- κ B-inducible transcription rates is 2. We chose this value because it is the same as the Hill coefficient in the NF- κ B-inducible transcription terms in the 2-feedback NF- κ B model on page 45 of the Supporting Online Material for Ashall et al. (2009).

The remaining dimensional parameters have values dependent on the nine reference concentrations defined at the start of Section 4. However, it is only necessary to estimate four of these reference concentrations because we can deduce from our choices for the non-dimensional parameters and the relationships between the dimensional and non-dimensional parameters that six of the reference concentrations are equal. For example, from (53) and since $A_{1,1}^* = A_{1,2}^*$ by (70), we trivially see that

$$[IKK\alpha]_{\text{ref}} = [IKK\alpha|IKK\alpha]_{\text{ref}}. \quad (87)$$

By similar observations involving the non-dimensional parameters in (70)–(73) and the parameter relationships in (53)–(64), we can quickly extend (87) to the following:

$$\begin{aligned} [IKK\alpha]_{\text{ref}} &= [IKK\alpha|IKK\alpha]_{\text{ref}} = [IKK\alpha|IKK\alpha|NF\kappa B]_{\text{ref}} \\ &= [IKK\alpha|NF\kappa B]_{\text{ref}} = [NF\kappa B]_{\text{ref}} = [IKK\alpha]_{\text{ref}}. \end{aligned} \quad (88)$$

We determine values for the reference concentrations in (88) by estimating $[IKK\alpha|NF\kappa B]_{\text{ref}}$. To do this, we first notice that a typical initial cytoplasmic concentration for $IKK\alpha|NF\kappa B$ used in the modelling literature is $0.08 \mu\text{M}$ (Ashall et al., 2009). Hence we can choose I_0 in (21) and (66) to equal $0.08 \mu\text{M}$. But then, by (66) and (74), we have

$$[IKK\alpha|NF\kappa B]_{\text{ref}} = \frac{I_0}{I_0^*} = 0.08 \mu\text{M}. \quad (89)$$

The reference concentrations not determined by (88) and (89) are $[IKK\alpha]_{\text{ref}}$, $[A20_t]_{\text{ref}}$, and $[A20]_{\text{ref}}$. We choose a value for $[IKK\alpha]_{\text{ref}}$ to be in line with the relative concentrations of mRNA and protein in non-dimensional units, as indicated in Fig. 6. This leads us to

$$[IKK\alpha]_{\text{ref}} = 0.032 \mu\text{M}. \quad (90)$$

We assume, as in Lipniacki et al. (2004) and Ashall et al. (2009), that the parameters governing NF- κ B-inducible synthesis of $IKK\alpha$ transcript are the same as for those governing synthesis of A20 transcript. Hence, in particular, we assume that $B_1 = B_2$, so that, by (58), (72), and (90), we see that

$$[A20_t]_{\text{ref}} = [IKK\alpha_t]_{\text{ref}} = 0.032 \mu\text{M}. \quad (91)$$

To find the last reference concentration, we assume, as in Lipniacki et al. (2004) and Ashall et al. (2009), that the translation

rates for $I\kappa B\alpha$ and A20 are the same, that is, $E_1 = E_2$. Then, by (62), (70), (88), (89), and (91), we have

$$[A20]_{\text{ref}} = [I\kappa B\alpha]_{\text{ref}} = 0.08 \mu\text{M}. \quad (92)$$

We can now calculate the remaining dimensional parameters. Using our values for the reference concentrations in (88)–(92) and our values for the non-dimensional parameters in (70)–(73), and also using (75), we find from the relationships in (53)–(64) that

$$A_1 = A_3 = 0.375(\mu\text{M})^{-1} \text{ s}^{-1}, \quad A_2 = 0.750(\mu\text{M})^{-1} \text{ s}^{-1}, \quad (93)$$

$$B_1 = B_2 = 0.0000128 \mu\text{M} \text{ s}^{-1}, \quad E_1 = E_2 = 0.0750 \text{ s}^{-1}, \quad (94)$$

$$F = 0.000320 \mu\text{M} \text{ s}^{-1}, \quad J = 1.25(\mu\text{M})^{-1} \text{ s}^{-1}, \quad M = 0.0052 \mu\text{M}. \quad (95)$$

Our values for the association rates A_1 , A_2 , and A_3 are consistent with fitted or assumed values for these parameters in other theoretical studies (Nelson et al., 2004; Hoffmann et al., 2002; Lipniacki et al., 2004). For example, in Lipniacki et al. (2004), the parameters a_2 , a_3 , and a_1 correspond to our parameters A_1 , A_2 , and A_3 , respectively, and are given values as follows: $a_2 = 0.2(\mu\text{M})^{-1} \text{ s}^{-1}$, $a_3 = 1(\mu\text{M})^{-1} \text{ s}^{-1}$, and $a_1 = 0.5(\mu\text{M})^{-1} \text{ s}^{-1}$.

Our values for the maximal transcription rates, B_1 and B_2 , are a little larger than the corresponding parameters, $c1a$ and $c1$, in the Supporting Online Material for Ashall et al. (2009). Furthermore our parameter M (concentration of NF- κ B at which NF- κ B-inducible transcription is half-maximal) is approximately one order of magnitude smaller than the corresponding parameter, namely k , in Ashall et al. (2009). However, this does not make our average transcription rates inconsistent with those in Ashall et al. (2009). Our parameter differences with Ashall et al. (2009) balance each other, since transcription is proportional to B_1 and B_2 but inversely proportional to M .

Our translation rates, E_1 and E_2 , are of roughly the same order of magnitude as corresponding parameters in Lipniacki et al. (2004) and Ashall et al. (2009). Our parameter F has no equivalent in the literature as far as we are aware, which is perhaps to be expected given that it is representative of a process (IKK activation) and not a single interaction. The parameter J in our model is in different units to the corresponding parameter in previous temporal studies (such as k_2 in Lipniacki et al., 2004), though it is not dissimilar in magnitude. We summarise our values for the dimensional parameters in Table 1.

Finally we have explored ranges of parameter values for which oscillations persist. By simulating the non-dimensionalised model (Eqs. (30)–(48)) with geometry as in Fig. 3 and with parameters determined by (67)–(74) except for the parameter being varied, we find oscillations with at least five distinct peaks in nuclear NF- κ B concentration for the following ranges:

$$0.0047 \leq D^* \leq 0.047, \quad (96)$$

$$0.0005 \leq d^* \leq 0.055, \quad (97)$$

$$0.0 \leq a^* \leq 24.0, \quad (98)$$

$$0.0 \leq H_2^* \leq 0.27. \quad (99)$$

Using the reference time in (75) and reference length in (77), we can convert the ranges in (96)–(99) to the following dimensional ranges:

$$0.0200 \mu\text{m}^2 \text{ s}^{-1} \leq D_X \leq 0.200 \mu\text{m}^2 \text{ s}^{-1}, \quad (100)$$

$$0.0000100 \text{ s}^{-1} \leq d_Y \leq 0.00110 \text{ s}^{-1}, \quad (101)$$

$$0.0 \mu\text{m} \text{ s}^{-1} \leq a_Z \leq 7.00 \mu\text{m} \text{ s}^{-1}, \quad (102)$$

$$0.0 \mu\text{m} \leq H_2 \leq 3.94 \mu\text{m}, \quad (103)$$

where X represents any of the species in the model, Y represents IKKa, $I\kappa B\alpha$ transcript, $I\kappa B\alpha$, A20 transcript, and A20, and Z represents $I\kappa B\alpha|NF\kappa B$, NF- κ B, and $I\kappa B\alpha$. Note that the range for the diffusion coefficient in (100) covers one order of magnitude. Similarly large ranges were found for diffusion coefficients in the two recent spatio-temporal models of intracellular pathways mentioned above (Terry et al., 2011; Sturrock et al., 2011).

The nature of the oscillatory dynamics varies across the ranges in (100)–(103). We discuss this below in relation to the parameter D_X (see Fig. 11 and comments on it in Section 5.1) and also in relation to the parameter H_2 (see Fig. 14 and comments on it in Section 5.2).

5.1. Analysis of numerical results

Figs. 4–6 show plots of total concentration over time for all species, created from a simulation of the non-dimensionalised model (Eqs. (30)–(48)) on the geometry depicted in Fig. 3 and with the parameter choices in (67)–(74). After continuous cell stimulation begins, all species quickly settle into stable oscillatory dynamics. This should not surprise us because each species is controlled in some way by a negative feedback loop at the core of the model (Fig. 2).

From Fig. 4(a), we see that for the species IKKa and $I\kappa B\alpha|NF\kappa B$ the total concentration exhibits a tall, narrow peak immediately after the onset of cell stimulation and is subsequently low. Such behaviour is consistent with the simulation results in Figs. 3 and 4 in Lipniacki et al. (2004) and with experimental results in Lee et al. (2000).

There is significantly more A20 than $I\kappa B\alpha$ (Figs. 4 and 6), even though both of these proteins have NF- κ B-inducible genes. This is because, in our model, $I\kappa B\alpha$ is lost by natural and catalytic degradation and by forming complexes with NF- κ B whereas A20 is lost only by natural degradation. To balance the levels of A20 and $I\kappa B\alpha$, Lipniacki et al. have assumed that A20 has a higher natural degradation rate than $I\kappa B\alpha$ but suggested that there may be a catalytic mechanism for A20 degradation that had not yet been discovered (Lipniacki et al., 2004). For more recent comments on the possible mechanisms by which A20 may be catalytically graded, see Coornaert et al. (2008). We have assumed that A20 and $I\kappa B\alpha$ have the same natural degradation rates, and it is clear by our description of Fig. 9 and our animations below that this assumption does not prevent our model from faithfully capturing observed spatio-temporal dynamics of the NF- κ B pathway.

The liberation of NF- κ B is notably greater during the first period of oscillations than in later periods (Fig. 5), which is in agreement with previous theoretical and experimental studies (Hoffmann et al., 2002; Nelson et al., 2004; Lipniacki et al., 2004; Ashall et al., 2009).

The total concentration of nuclear $I\kappa B\alpha|NF\kappa B$ oscillates in a qualitatively different fashion to all the other species, with twice as many peaks (Fig. 5, middle). As far as we are aware, this is not a behaviour that has been seen in previous models based on ordinary differential equations (ODEs) or delay differential equations (DDEs). We suggest an explanation for this “double peak” behaviour by first noting that nuclear $I\kappa B\alpha|NF\kappa B$ is formed when nuclear $I\kappa B\alpha$ and nuclear NF- κ B bind together. It is then clear, from inspecting Figs. 5 and 6, that the successive peaks in nuclear $I\kappa B\alpha|NF\kappa B$ follow peaks in nuclear NF- κ B and nuclear $I\kappa B\alpha$, respectively. It is to be expected that peaks in nuclear $I\kappa B\alpha$ will occur after and not coincide with peaks in nuclear NF- κ B, since NF- κ B is a transcription factor for $I\kappa B\alpha$ —it will take time for $I\kappa B\alpha$ to be synthesised in the cytoplasm and translocate to the nucleus

once its gene has been activated by nuclear NF- κ B. Our explanation seems quite satisfactory until we bear in mind that a similar argument involving peaks in cytoplasmic NF- κ B and I κ B α would predict twice as many peaks in cytoplasmic I κ B α |NF κ B as are observed. However, this need not trouble us because it would be insufficient to rely on such reasoning alone to explain the source of cytoplasmic I κ B α |NF κ B. In our model, nuclear I κ B α |NF κ B is actively transported to the cytoplasm. Moreover the peaks in cytoplasmic I κ B α |NF κ B are fairly rounded.

Experimental data in Rice and Ernst (1993) and considerations in Carloti et al. (2000) indicate that unbound I κ B α (that is, I κ B α not complexed to other species) constitutes less than 15% of the total I κ B α . Our results are in agreement with this, showing that the vast majority of I κ B α is found in complexes with NF- κ B in the cytoplasm.

Spatial profiles of NF- κ B, I κ B α |NF κ B, I κ B α transcript, and I κ B α are presented over a typical period in Figs. 7 and 8. From these figures, we notice that newly liberated cytoplasmic NF- κ B translocates to the nucleus (times 420, 440, 460), where it causes production of I κ B α transcript (times 440, 460, 480). The production of I κ B α transcript leads to translation of I κ B α in the cytoplasm (times 460, 480, 500). This new I κ B α is actively transported to the nucleus where it binds to NF- κ B, sequestering it in the complex I κ B α |NF κ B, which is then actively transported out into the cytoplasm (times 480, 500).

A significant proportion of the NF- κ B liberated in the cytoplasm does not enter the nucleus (Fig. 5). This may seem biologically counter-intuitive given the importance of NF- κ B as a transcription factor. But notice that the local concentration of NF- κ B in the nucleus attains a higher peak because the nucleus has a smaller volume than the cytoplasm (times 440, 460, 480 in Fig. 7). Why should it be that not all of the liberated NF- κ B enters the nucleus in our results? The answer is clear from times 440 and 460 in Figs. 7(a) and 8. I κ B α transcript production begins when the first newly liberated NF- κ B enters the nucleus, leading to I κ B α production in the cytoplasm before all of the liberated NF- κ B can translocate to the nucleus. The newly synthesised I κ B α then binds to some of the liberated NF- κ B before it reaches the nucleus.

Spatial profiles of the main NF- κ B-containing species (I κ B α |NF κ B+NF- κ B) are shown over the first period in Fig. 9(a) and over a typical period in Fig. 9(b). Since most of the NF- κ B is liberated during the first period and is actively transported to the nucleus (Fig. 5), the bulk of the main NF- κ B-containing species moves from the cytoplasm to the nucleus (times 100, 120, 140 in Fig. 9(a)). NF- κ B-inducible production of I κ B α then leads to NF- κ B being again sequestered in the cytoplasm in the complex I κ B α |NF κ B (times 160, 180, 200 in Fig. 9(a)). A smaller proportion of NF- κ B is liberated during subsequent periods because there is relatively little IKK α to drive this after the first period (Fig. 4(a)). Hence, although the NF- κ B-containing species (in the form of liberated NF- κ B) continue to periodically enter the nucleus (times 440, 460, 480 in Fig. 9(b)), there is always a noticeable quantity of these species in the cytoplasm (all times in Fig. 9(b)).

The behaviour demonstrated in Fig. 9 is exactly the same as that demonstrated in the experimental results (reproduced from Nelson et al., 2004) in Fig. 1. The time information in Figs. 1 and 9 does not exactly correspond—for example, stimulation begins at time 0 in Fig. 1 but at time 100 in Fig. 9. Hence the equivalence of the behaviour can be seen from comparing times 100, 120, 140, and 200 in Fig. 9(a) with times 0, 6, 60, and 120, respectively, in Fig. 1, and from comparing times 400, 460, and 500 in Fig. 9(b) with times 300, 380, and 410, respectively, in Fig. 1.

Movie clips involving red fluorescent-tagging of NF- κ B and showing the behaviour of the NF- κ B-containing species in living cells are included as Supporting Online Material for Nelson et al. (2004). The images from Fig. 1 are snapshots from one of these

movies, namely movie clip S1. We include animations from our computational results as Supporting Information files. In particular, animation S3 shows the main NF- κ B-containing species and bears a striking resemblance to movie clip S1 from Nelson et al. (2004). For further details, see the section below called “Supporting Information”.

When all the active transport rates are set equal to zero, as in Fig. 10(a), then oscillatory dynamics still occur. Hence diffusive transport alone is sufficient for oscillations. However, by comparing Fig. 10(a) with Fig. 5, we see that the removal of active transport causes the oscillations in nuclear NF- κ B to have a smaller amplitude, causes the total concentration of nuclear NF- κ B to remain positive instead of dropping to zero between successive peaks, and causes the “double peak” feature of nuclear I κ B α |NF κ B to be lost.

The model dynamics are changed more dramatically when NF- κ B is actively transported towards the nucleus throughout the cytoplasm. Fig. 10(b) was made in the same way as Fig. 5 with active transport of NF- κ B, I κ B α , and I κ B α |NF κ B across the nuclear membrane at $0.438 \mu\text{m s}^{-1}$, but additionally there is now active transport of cytoplasmic NF- κ B towards the nucleus and also at $0.438 \mu\text{m s}^{-1}$. This latter transport could represent facilitated movement along cytoskeletal elements called microtubules. At least in neuronal cells, which possess an elongated morphology that poses a particular challenge to intracellular signal transduction, experiments have shown that NF- κ B-dependent transcriptional activity is reduced by microtubule-disrupting drugs (Mackenzie et al., 2006; Mikenberg et al., 2007). Clearly the inclusion of cytoplasmic active transport of NF- κ B in Fig. 10(b) causes oscillatory dynamics to be lost and more NF- κ B to remain in the nucleus. We have found (results not shown) that oscillations in NF- κ B can occur when there is cytoplasmic active transport of NF- κ B but only when the rate of this transport is less than $0.0350 \mu\text{m s}^{-1}$. In any case, given the importance of NF- κ B as a transcription factor, with hundreds of target genes, it is clear by comparing Figs. 5 and 10(a) and (b) that the mechanisms by which a cell transports NF- κ B to the nucleus will significantly influence how it responds to activation of its NF- κ B pathway. The ability to properly distinguish between different modes of transport, such as diffusion and active transport, is an inherent feature of a spatio-temporal modelling approach that is not shared by traditional compartmental ODE or DDE models.

As mentioned at the beginning of Section 5, we have assumed for simplicity that the diffusion coefficient D_X is the same for all species X. In Eq. (100), we noted that our model yields at least five distinct peaks in nuclear NF- κ B activity for $0.0200 \mu\text{m}^2 \text{s}^{-1} \leq D_X \leq 0.200 \mu\text{m}^2 \text{s}^{-1}$. Fig. 11 shows how the time evolution of the total concentration of cytoplasmic and nuclear NF- κ B varies with D_X . We see that the amplitude of the oscillations in nuclear NF- κ B is greatest when $D_X = 0.0425 \mu\text{m}^2 \text{s}^{-1}$, the oscillatory period is reduced as D_X increases, and the total amount of NF- κ B (cytoplasmic plus nuclear) is also reduced as D_X increases. Fig. 11 gives an indication of the robustness of oscillatory dynamics to variety in D_X . Such robustness is encouraging because oscillatory dynamics are known to occur in living cells (Fig. 1) yet not all the species in our model will, in reality, have the same diffusion coefficient. For example, proteins are larger than transcript molecules and therefore diffuse more slowly. We hope that this work will motivate experimentalists to measure the diffusion coefficients for all of the species in the NF- κ B pathway. As measurements become available, we will incorporate them into our spatio-temporal modelling framework and confirm or improve our predictions.

5.2. Influence of cell geometry on NF- κ B dynamics

From Fig. 1 and movie clips in the Supporting Online Material for Nelson et al. (2004), we see that cells can change shape on the

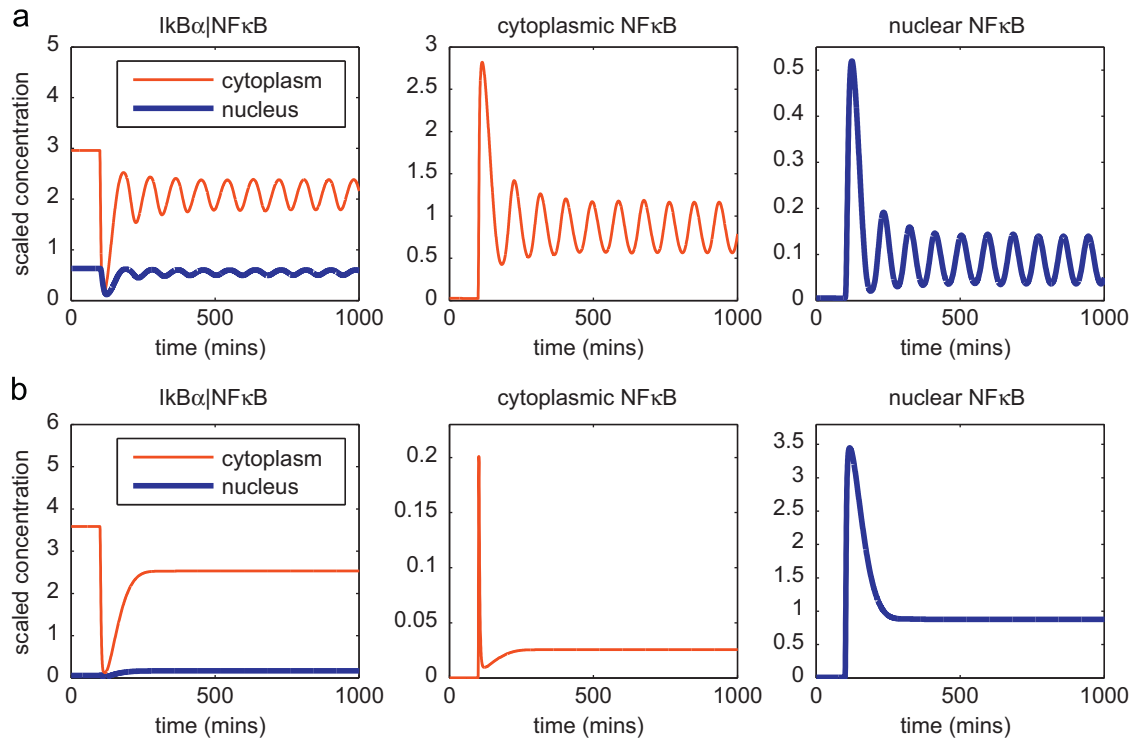


Fig. 10. (a) Plots showing the total concentration over time for $I\kappa B\alpha|NF\kappa B$ and $NF\kappa B$ created from a simulation of the non-dimensionalised model (Eqs. (30)–(48)), with geometry as in Fig. 3 and model parameters determined by (67)–(74), except that all active transport rates are set equal to zero. Continuous cell stimulation begins at 100 min and concentrations are shown in non-dimensional units. The plots in (b) were created in the same way as in (a) except that active transport was permitted across the nuclear membrane and additionally $NF\kappa B$ was assumed to be actively transported through the cytoplasm towards the nuclear membrane, where all active transport rates satisfy (67) and (69).

same timescale as oscillatory nuclear-cytoplasmic translocation of $NF\kappa B$. Hence in this subsection we have explored the impact on $NF\kappa B$ oscillations of variety in cell geometry in our model. Fig. 12 shows that sustained oscillations in $NF\kappa B$ can occur when the nucleus is off-centre or when the cell is elliptical. However, they do not occur (at least for the parameter set which we are using) when the cell is particularly flat. For each simulation in Fig. 12 the geometry is static. In future work we will be interested in creating simulations during which the cell geometry changes. Above all, we will ask if oscillatory dynamics may persist if the cell becomes flat but only briefly.

Fig. 13 shows that sustained oscillations in $NF\kappa B$ can occur when the nucleus is elliptical or large (relative to the cell). Yet oscillations are lost when the nucleus is significantly reduced in size. How do we account for this? Recall that the total amount of $NF\kappa B$ -containing species is constant in our model and is initially contained entirely in cytoplasmic $I\kappa B\alpha|NF\kappa B$ complexes. From the initial condition in (74), it is clear that the initial total amount of $I\kappa B\alpha|NF\kappa B$ will be greater if the cytoplasm contains more space. Hence, if we decrease the size of the nucleus without changing the size of the cell, then more $NF\kappa B$ can be liberated in response to external stimulation. However, the $NF\kappa B$ -inducible production of $I\kappa B\alpha$ transcript is a saturating function of $NF\kappa B$. Therefore, an increase in liberated $NF\kappa B$ will not necessarily lead to a corresponding increase in $I\kappa B\alpha$. In addition, we have assumed that transcription can occur anywhere in the nucleus rather than at specific sites (genes), so that a smaller nucleus will reduce transcription rates. Thus, for a sufficiently small nucleus (such as in the top row of Fig. 13), the negative feedback inhibition by $I\kappa B\alpha$ becomes so limited relative to the amount of liberated $NF\kappa B$ that most of the $NF\kappa B$ remains liberated without being sequestered again in the cytoplasm in the complex $I\kappa B\alpha|NF\kappa B$.

Our model would clearly be more realistic if we were to assume that transcription can only be produced at specific sites (genes) within the nucleus rather than everywhere in it. Our assumptions are appropriate, however, for a first step in the spatio-temporal modelling of the $NF\kappa B$ pathway. In future work we will consider transcription at specific sites in the nucleus. We will moreover investigate how the location of genes influences their sensitivity to transcription factors. Experimental studies have already revealed connections between the locations of genes and their activation (Cole and Scarcelli, 2006).

Finally, we comment on the robustness of oscillatory dynamics in our model to changes in the minimum distance H_2 of translation from the nuclear membrane. Earlier (Eq. (103)) we noted that there are at least five distinct peaks in the total concentration of nuclear $NF\kappa B$ for $0.0 \mu m \leq H_2 \leq 3.94 \mu m$. The behaviour of $NF\kappa B$ for various values of H_2 is demonstrated in Fig. 14. It is evident from this figure that the proportion of $NF\kappa B$ that enters the nucleus increases with H_2 . Also, the amplitude of the oscillations in nuclear $NF\kappa B$ is greatest for $H_2 \approx 2.92 \mu m$ and the period increases with H_2 (for those values of H_2 that yield oscillations). The biological implication of these results is that the response of a cell to activation of its $NF\kappa B$ pathway will be sensitive to the spatial arrangement of its translational machinery.

Proteins are translated at ribosomes which are either free in the cytosol or which associate with the endoplasmic reticulum (ER), a netlike labyrinth of tubules and flattened sacs that surrounds the nuclear membrane and extends into the cytosol. Typically proteins used in the cell, such as $I\kappa B\alpha$, are translated at free ribosomes whilst those intended for export or use at the cell membrane are processed in the ER (Alberts et al., 2008, p. 724). In any case, the size and extent of the ER will clearly influence the location of either free ribosomes or of those which associate with it.

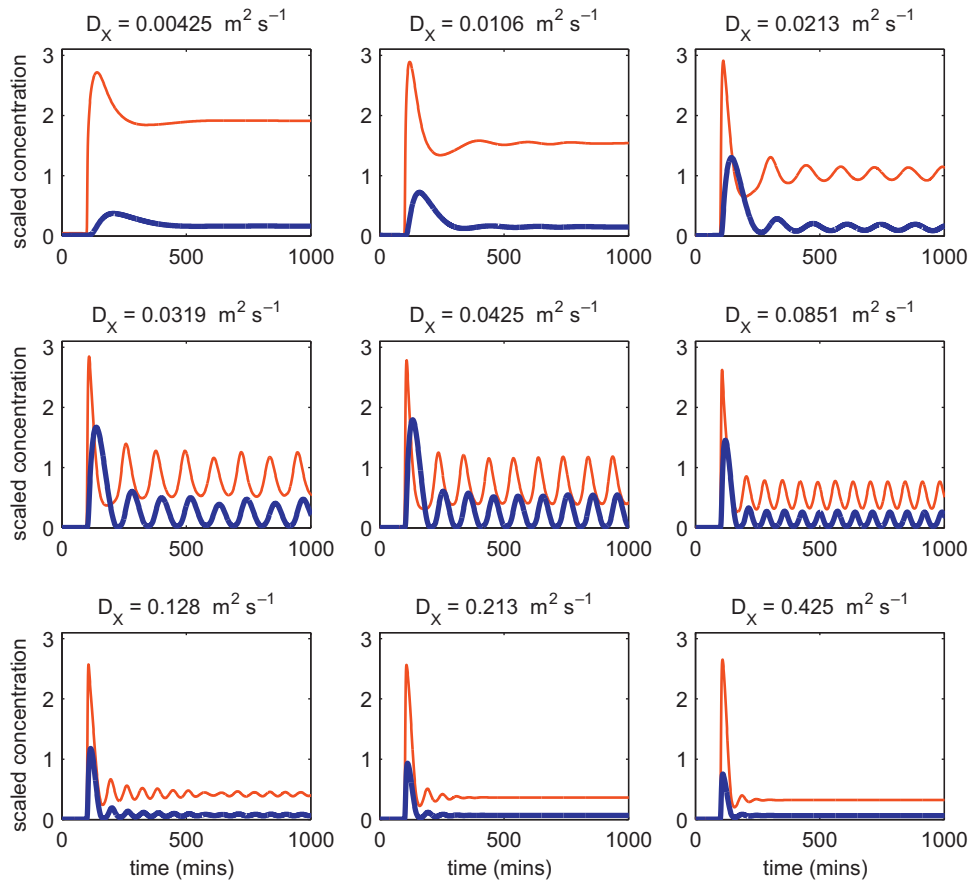


Fig. 11. Plots showing total NF- κ B concentration over time in the cytoplasm (thin red lines) and nucleus (thick blue lines) created from simulations of the non-dimensionalised model (Eqs. (30)–(48)), with geometry as in Fig. 3 and parameters determined by (67)–(74), except for the parameter D^* which takes a different value in each plot. In the top row (left to right), $D^* = 0.001, 0.0025, 0.005$; in the second row, $D^* = 0.0075, 0.01, 0.02$; and in the third row, $D^* = 0.03, 0.05, 0.1$. The title of each plot shows the dimensional equivalent of D^* , namely the diffusion coefficient D_X of every species X , calculated by the same method used in (80). Continuous cell stimulation begins at 100 min. Concentrations are shown in non-dimensional units. (For interpretation of the references to colour in this figure legend, the reader is referred to the web version of this article.)

There appears to be little published experimental data on the spatio-temporal interactions of the ER, free ribosomes, and intracellular signalling pathways, perhaps because it is difficult to accurately measure these interactions. It may also be because the mathematical framework for employing spatio-temporal data is still developing (Terry et al., 2011; Sturrock et al., 2011). Without a suitable modelling framework, such data has limited use and is unlikely to yield reliable predictions. We hope that by our creation and exploration of an initial model for the spatio-temporal dynamics of the NF- κ B pathway, experimentalists will choose to explore the issues raised in this work, confident that their data can be given a meaningful analysis.

6. Discussion

Given the existence of experimental evidence indicating that cell size and shape can significantly influence intracellular signal transduction (Meyers et al., 2006; Neves et al., 2008), we have created a spatio-temporal model of partial differential equations for the NF- κ B signalling pathway. Our modelling assumptions are similar to those in Lipniacki et al. (2004) with several exceptions: we explicitly model molecular movement by diffusion and active transport, and (as in Ashall et al., 2009) we represent NF- κ B-inducible transcription as a saturating function of NF- κ B. Our model contains two activators, IKK α and NF- κ B, and two NF- κ B-inducible inhibitors, I κ B α and A20.

The NF- κ B pathway is known to exhibit oscillatory dynamics (Nelson et al., 2004; Krishna et al., 2006; Friedrichsen et al., 2006). Through numerical simulations of our model, we have found parameter values such that sustained oscillations occur. Our values are consistent with experimental measurements for those parameters for which such measurements exist. For rates of diffusion, active transport, and degradation, we have found ranges of values such that oscillations persist.

Consistent with previous theoretical and experimental studies (Lipniacki et al., 2004; Lee et al., 2000), we found that, after the onset of continuous cell stimulation, IKK activity peaks quickly but is subsequently low. Curiously, we found that nuclear I κ B α |NF κ B oscillates with twice as many peaks as nuclear I κ B α and nuclear NF- κ B. This prediction does not appear to have been made by previous mathematical models of the NF- κ B pathway. We linked this “double peak” behaviour to two facts: first, I κ B α |NF κ B forms in the nucleus when I κ B α and NF- κ B associate there; second, peaks in nuclear I κ B α necessarily follow peaks in nuclear NF- κ B since NF- κ B is a transcription factor for I κ B α .

Our model also predicted that not all of the NF- κ B liberated by cell stimulation will translocate to the nucleus. Plots of spatial profiles suggested that NF- κ B liberated near the cell membrane may be sequestered in the cytoplasm by newly synthesised I κ B α before reaching the nucleus. Plots of the main NF- κ B-containing species in our model (Fig. 9) were found to strikingly resemble corresponding experimental images of a fluorescent fusion protein in Nelson et al. (2004) (reproduced in Fig. 1), justifying our

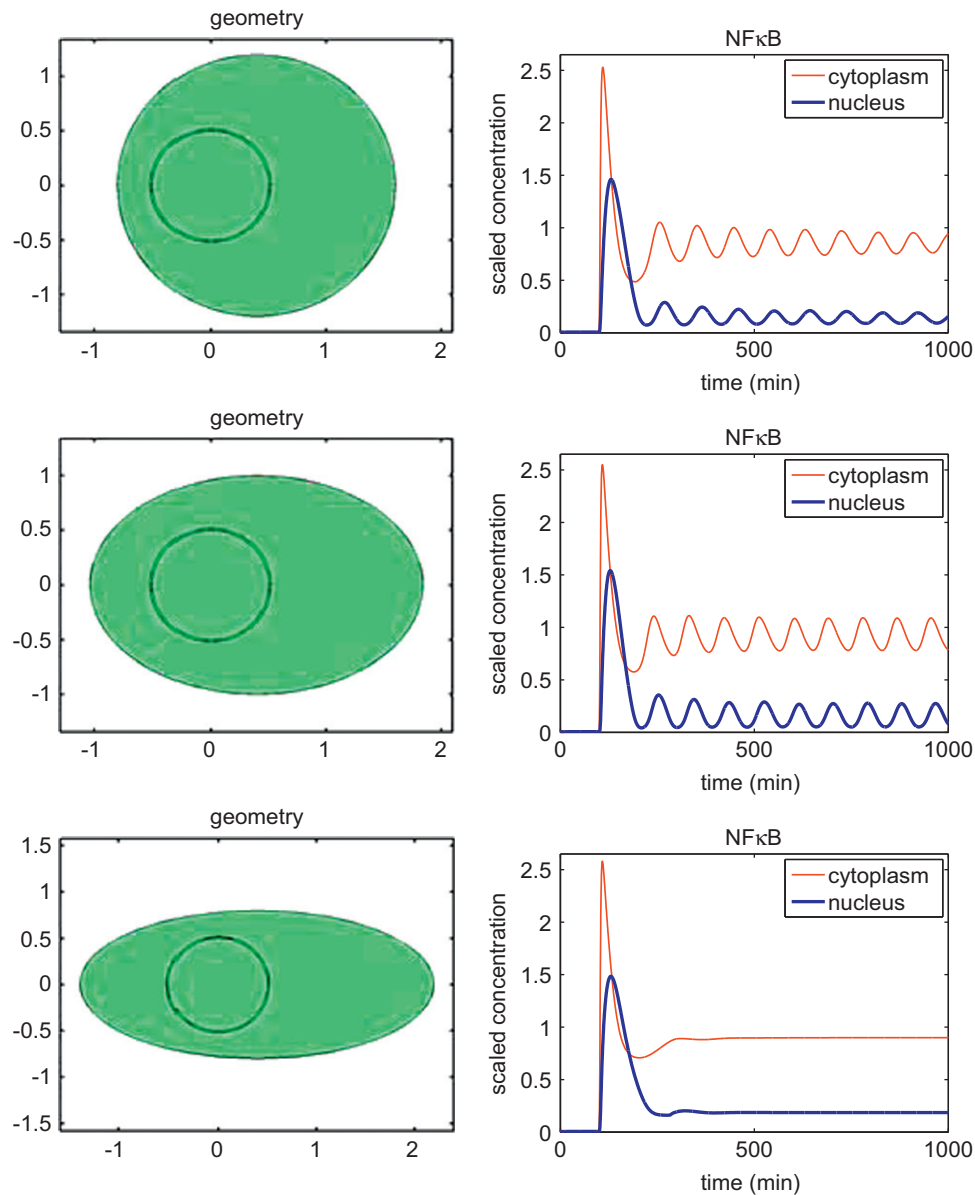


Fig. 12. Plots showing total NF- κ B concentration over time created from simulations of the non-dimensionalised model (Eqs. (30)–(48)) with parameters determined by (67)–(74). Continuous cell stimulation begins at 100 min. Each row shows the geometry on which a simulation is performed, with the corresponding numerical results to the right of each geometry. The nucleus is the same in each geometry and is located to the left of the cell—here we vary the shape of the cell whilst keeping its total area the same as in Fig. 3. Concentrations are shown in non-dimensional units.

spatio-temporal approach. Animations created from our numerical solution also strongly resemble corresponding experimental movie clips in Nelson et al. (2004), further justifying our approach (see the Supporting Information section below).

We modelled active transport as convection across the nuclear membrane, physiologically representing facilitated transport through nuclear pore complexes. Three species were subject to active transport—NF- κ B and I κ B α were transported *into* the nucleus since they possess nuclear import sequences (Mackenzie et al., 2006; Mikenberg et al., 2007; Sachdev et al., 1998) and I κ B α |NF- κ B was transported *out* of the nucleus since it has a nuclear export sequence (Arenzana-Seisdedos et al., 1997). When we set all active transport rates to zero, we found that sustained oscillatory dynamics still occur. However, the character of the oscillations in nuclear NF- κ B was changed, for example by a reduction in their amplitude. By contrast, when we assumed, in view of evidence from neuronal cells (Mackenzie et al., 2006; Mikenberg et al., 2007), that NF- κ B could be actively transported

throughout the cytoplasm towards the nucleus (with active transport permitted across the nuclear membrane for NF- κ B, I κ B α , and I κ B α |NF- κ B), oscillations were lost and the total concentration of nuclear NF- κ B was notably increased. Given that NF- κ B is a transcription factor with hundreds of target genes (Alberts et al., 2008), it seems clear by our results that the mechanisms by which a cell transports NF- κ B to the nucleus will significantly influence how it responds to activation of its NF- κ B pathway.

The explicitly spatial modelling framework adopted in this paper has allowed us to address questions not amenable to compartmental models of ordinary or delay differential equations. By considering a variety of cell geometries, we have found that sustained oscillations in NF- κ B are robust to changes in the shape of the cell or the shape, size, and location of its nucleus. However, we noticed that oscillations are lost when the cell is particularly flat or the nucleus sufficiently reduced in size. Since cells can change shape on the same timescale as oscillatory nuclear-cytoplasmic

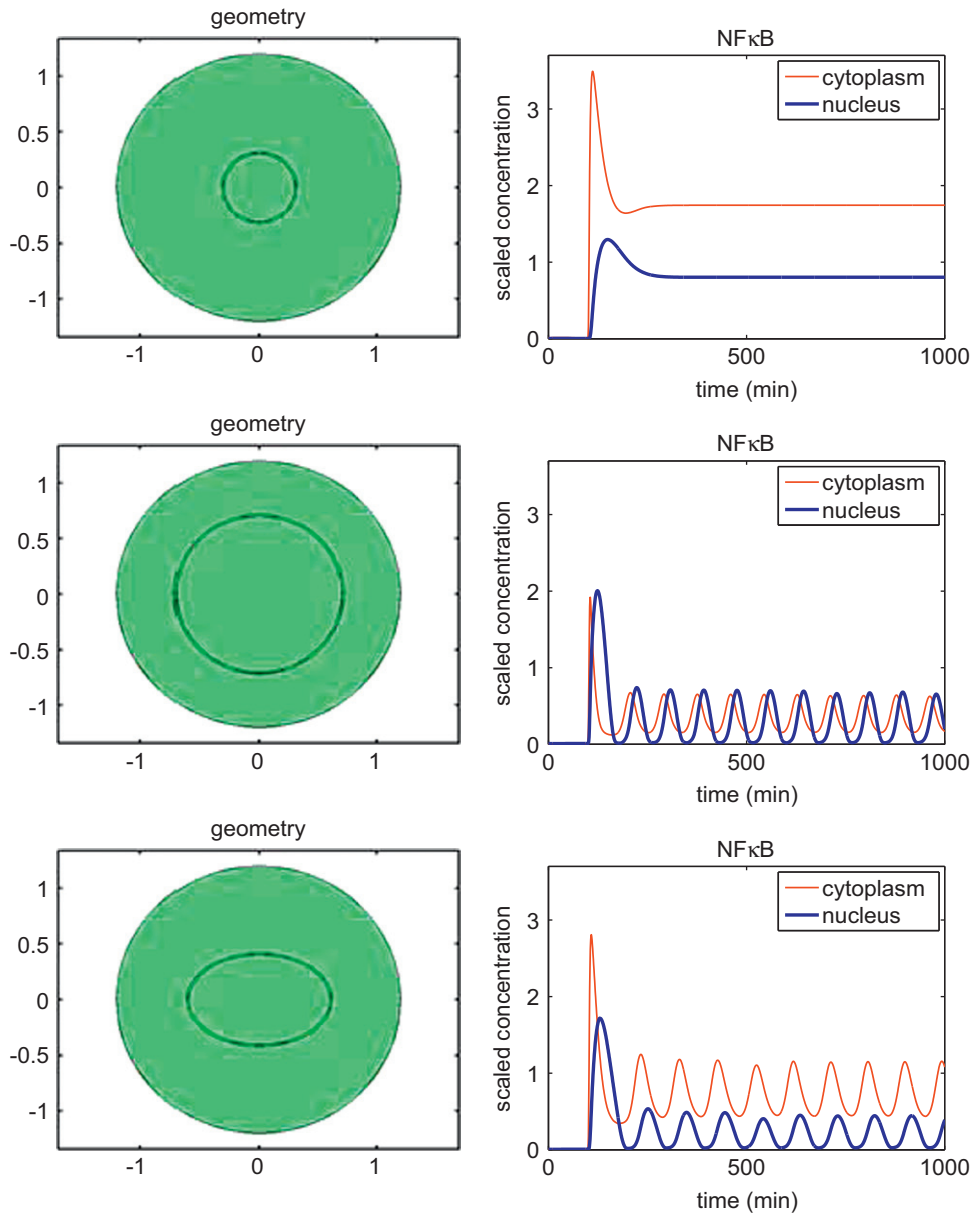


Fig. 13. Plots showing total NF- κ B concentration over time created from simulations of the non-dimensionalised model (Eqs. (30)–(48)) with parameters determined by (67)–(74). Continuous cell stimulation begins at 100 min. Each row shows the geometry on which a simulation is performed, with the corresponding numerical results to the right of each geometry. In each geometry the cell shape and size is the same as in Fig. 3—here we vary only the size or shape of the nucleus. Concentrations are shown in non-dimensional units.

translocation of NF- κ B (Fig. 1), we will, in future work, create simulations with an evolving cell geometry.

We were able to control the distance from the nucleus at which translation of proteins from ribosomes occurs. We found that if the minimum distance of translation from the nuclear membrane is larger, then a larger proportion of NF- κ B enters the nucleus and that there is a value (approximately $2.9 \mu\text{m}$) for this minimum distance which maximises the amplitude of oscillations in nuclear NF- κ B. With the continuing advance of imaging technology leading to new experimental measurements of rates of diffusion and active transport (Seksek et al., 1997; Klonis et al., 2002; Matsuda et al., 2008), we anticipate that the value of our spatio-temporal modelling approach will become even more apparent.

Although the spatio-temporal modelling of individual intracellular signalling pathways is certainly insightful, it should be borne in mind that different signalling pathways inside a cell

often interact. Hence a more complete picture of the functioning of a cell could be attained by the construction and analysis of spatio-temporal models of several interacting pathways. It is already known that NF- κ B can both co-operate with and antagonise another pathway that is also important in controlling apoptosis, innate and adaptive immune responses, and inflammation, namely the p53 pathway (Pommier et al., 2004; Perkins, 2007). A temporal study of crosstalk between these pathways has been conducted (Puszynski et al., 2009) but, as yet, no spatio-temporal study has appeared.

Transcriptional control systems are subject to stochastic effects, so as future work we shall incorporate stochasticity into our model, possibly by utilising the Gillespie algorithm (Barik et al., 2008, 2010; Kar et al., 2009). We also intend to further this work by asking what happens when transcription occurs only at specific locations (genes) in the nucleus, rather than at all points in the nucleus as assumed in our model. In addition, we may extend our

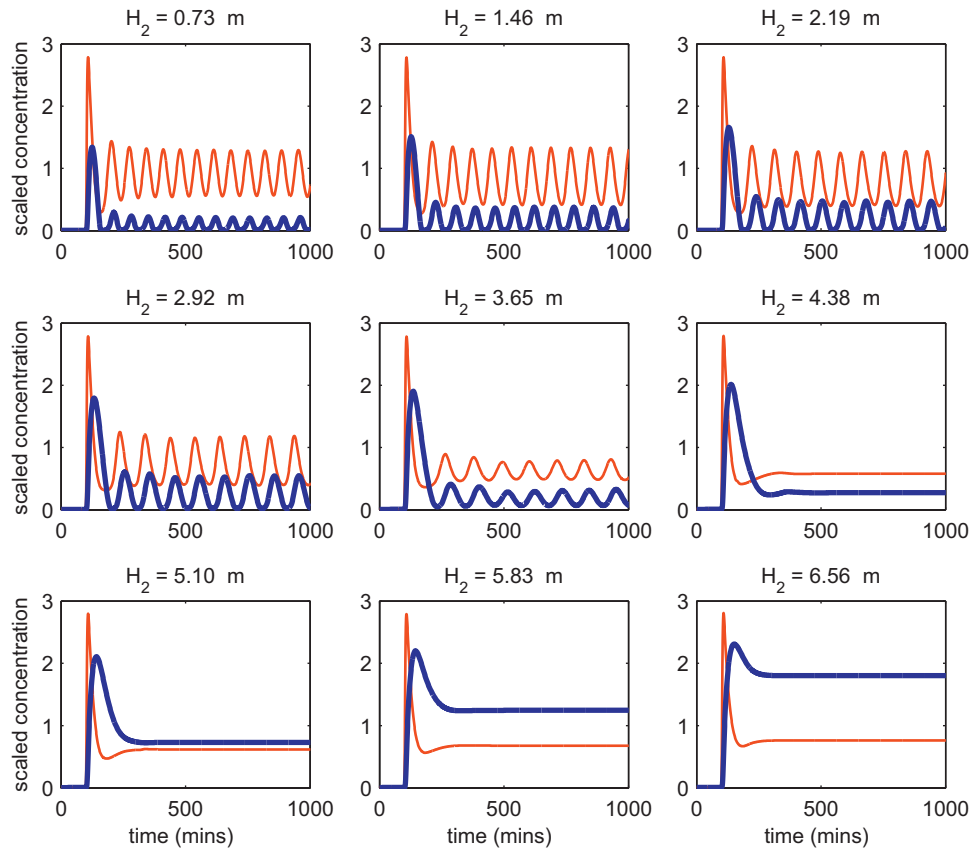


Fig. 14. Plots showing total NF- κ B concentration over time in the cytoplasm (thin red lines) and nucleus (thick blue lines) created from simulations of the non-dimensionalised model (Eqs. (30)–(48)), with geometry as in Fig. 3 and parameters determined by (67)–(74), except for the parameter H_2^* which takes a different value in each plot. In the top row (left to right), $H_2^* = 0.05, 0.1, 0.15$; in the second row, $H_2^* = 0.2, 0.25, 0.3$; and in the third row, $H_2^* = 0.35, 0.4, 0.45$. The title of each plot shows the dimensional equivalent of H_2^* , namely the minimum distance H_2 of translation from the nuclear membrane, calculated by the same method used in (79). The proportion of liberated NF- κ B that enters the nucleus grows with H_2 . Continuous cell stimulation begins at 100 min. Concentrations are shown in non-dimensional units. (For interpretation of the references to colour in this figure legend, the reader is referred to the web version of this article.)

model by including species upstream of IKK activation. Finally it would be worth investigating pulsatile cell stimulation (Ashall et al., 2009) as opposed to the continuous stimulation considered here, and we will, in future work, incorporate targeted drug therapy into our model, since the NF- κ B pathway is found to be constitutively active in a number of human cancers (Weinberg, 2007).

Supporting Information

Animations S1, S2, S3, and S4: Animations of (S1) NF- κ B concentration, (S2) I κ B α concentration, (S3) I κ B α |NF- κ B+NF- κ B concentration, and (S4) I κ B α |NF- κ B+I κ B α concentration created from a simulation of the non-dimensionalised model (Eqs. (30)–(48)) with geometry as in Fig. 3 and parameters determined by (67)–(74). Time is shown in non-dimensional units. Cell stimulation begins at 300 time units. Concentrations are in non-dimensional units.

Animation S3 shows the main NF- κ B-containing species in our model and bears a strong resemblance to corresponding experimental movie clips of NF- κ B-containing species fused to a red fluorescent protein in the Supporting Online Material for Nelson et al. (2004) (for example, see movie clip S1). Animation S4 shows the main I κ B α -containing species in our model and bears a strong resemblance to corresponding experimental movie clips of I κ B α -containing species fused to a green fluorescent protein in the Supporting Online Material for Nelson et al. (2004) (for example, see movie clips S1 and S2).

Supplementary material related to this article can be found online at doi:10.1016/j.jtbi.2011.08.036.

Acknowledgements

The authors gratefully acknowledge the support of the ERC Advanced Investigator Grant 227619, “M5CGS—From Mutations to Metastases: Multiscale Mathematical Modelling of Cancer Growth and Spread”.

References

- Alberts, B., Johnson, A., Lewis, J., Raff, M., Roberts, K., Walter, P., 2008. *Molecular Biology of the Cell*, fifth ed. Garland Science, Taylor & Francis Group, LLC.
- Arenzana-Seisdedos, F., Turpin, P., Rodriguez, M., Thomas, D., Hay, R., Virelizier, J., Dargemont, C., 1997. Nuclear localization of I κ B α promotes active transport of NF- κ B from the nucleus to the cytoplasm. *J. Cell Sci.* 110, 369–378.
- Ashall, L., Horton, C., Nelson, D., Paszek, P., Harper, C., Sillitoe, K., Ryan, S., Spiller, D., Unitt, J., Broomhead, D., Kell, D., Rand, D., See, V., White, M., 2009. Pulsatile stimulation determines timing and specificity of NF- κ B-dependent transcription. *Science* 324, 242–246.
- Bar-Or, R.L., Maya, R., Segel, L., Alon, U., Levine, A., Oren, M., 2000. Generation of oscillations by the p53-mdm2 feedback loop: a theoretical and experimental study. *Proc. Natl. Acad. Sci. USA* 97, 11250–11255.
- Barik, D., Baumann, W.T., Paul, M.R., Novak, B., Tyson, J.J., 2010. A model of yeast cell-cycle regulation based on multisite phosphorylation. *Mol. Sys. Biol.* 6, 405.
- Barik, D., Paul, M.R., Baumann, W.T., Cao, Y., Tyson, J.J., 2008. Stochastic simulation of enzyme-catalyzed reactions with disparate timescales. *Biophys. J.* 95, 3563–3574.
- Bernard, S., Cajavec, B., Pujol-Menjouet, L., Mackey, M., Herzel, H., 2006. Modelling transcriptional feedback loops: the role of Gro/TLE1 in Hes1 oscillations. *Philos. Trans. R. Soc. A* 364, 1155–1170.

- Brown, G., Kholodenko, B., 1999. Spatial gradients of cellular phospho-proteins. *FEBS Lett.* 457, 452–454.
- Carlotti, F., Dower, S., Qvarnstrom, E., 2000. Dynamic shuttling of nuclear factor κ B between the nucleus and cytoplasm as a consequence of inhibitor dissociation. *J. Biol. Chem.* 275, 41028–41034.
- Chang, H., Kim, M., Baek, M., Park, J., Chung, I., Shin, B., Ahn, B., Jung, Y., 2007. Triptolide inhibits tumor promoter-induced uPAR expression via blocking NF- κ B signaling in human gastric AGS cells. *Anticancer Res.* 27, 3411–3417.
- Cheong, R., Hoffmann, A., Levchenko, A., 2008. Understanding NF- κ B signaling via mathematical modeling. *Mol. Syst. Biol.* 4.
- Chung, C., Ely, K., McGavran, L., Varella-Garcia, M., Parker, J., Parker, N., Jarrett, C., Carter, J., Murphy, B., Netterville, J., Burkey, B., Sinard, R., Cmelak, A., Levy, S., Yarbrough, W., Slebos, R., Hirsch, F., 2006. Increased epidermal growth factor receptor gene copy number is associated with poor prognosis in head and neck squamous cell carcinomas. *J. Clin. Oncol.* 24 (25), 4170–4176.
- Cole, C., Scarcelli, J., 2006. Transport of messenger RNA from the nucleus to the cytoplasm. *Curr. Opin. Cell Biol.* 18, 299–306.
- Coornaert, B., Baens, M., Heynincx, K., Bekaert, T., Haegman, M., Staal, J., Sun, L., Chen, Z., Marynen, P., Beyaert, R., 2008. T cell antigen receptor stimulation induces MALT1 paracaspase-mediated cleavage of the NF- κ B inhibitor A20. *Nat. Immunol.* 9, 263–271.
- Dequeant, M., Glynn, E., Gaudenz, K., Wahl, M., Chen, J., Mushegian, A., Pourquie, O., 2006. A complex oscillating network of signaling genes underlies the mouse segmentation clock. *Science* 314, 1595–1598.
- Friedrichsen, S., Harper, C., Semprini, S., Wilding, M., Adamson, A., Spiller, D., Nelson, G., Mullins, J., White, M., Davis, J., 2006. Tumor necrosis factor- α activates the human prolactin gene promoter via nuclear factor- κ B signaling. *Endocrinology* 147, 773–781.
- Gordon, K., van Leeuwen, I., Lain, S., Chaplain, M., 2009. Spatio-temporal modelling of the p53-mdm2 oscillatory system. *Math. Model. Nat. Phenom.* 4, 97–116.
- Hat, B., Puszynski, K., Lipniacki, T., 2009. Exploring mechanisms of oscillations in p53 and nuclear factor- κ B systems. *IET Syst. Biol.* 3, 342–355.
- Hirata, H., Yoshiura, S., Ohtsuka, T., Bessho, Y., Harada, T., Yoshikawa, K., 2002. Oscillatory expression of the bHLH factor Hes1 regulated by a negative feedback loop. *Science* 298, 840–843.
- Hoffmann, A., Levchenko, A., Scott, M., Baltimore, D., 2002. The I κ B-NF- κ B signaling module: temporal control and selective gene activation. *Science* 298, 1241–1245.
- Kar, S., Baumann, W.T., Paul, M.R., Tyson, J.J., 2009. Exploring the roles of noise in the eukaryotic cell cycle. *Proc. Natl. Acad. Sci. USA* 106, 6471–6476.
- Kholodenko, B., 2006. Cell-signalling dynamics in time and space. *Nat. Rev. Mol. Cell Biol.* 7, 165–174.
- Klonis, N., Rug, M., Harper, I., Wickham, M., Cowman, A., Tilley, L., 2002. Fluorescence photobleaching analysis for the study of cellular dynamics. *Eur. Biophys. J.* 31, 36–51.
- Kokura, S., Yoshida, N., Ishikawa, T., Higashihara, H., Sakamoto, N., Takagi, T., Uchiyama, K., Naito, Y., Mazda, O., Okanoue, T., Yoshikawa, T., 2005. Interleukin-10 plasmid DNA inhibits subcutaneous tumor growth of Colon26 adenocarcinoma in mice. *Cancer Lett.* 218, 171–179.
- Krishna, S., Jensen, M., Sneppen, K., 2006. Minimal model of spiky oscillations in NF- κ B. *Proc. Natl. Acad. Sci. USA* 103, 10840–10845.
- Kruger, R., Heinrich, R., 2004. Model reduction and analysis of robustness for the Wnt/ β -catenin signal transduction pathway. *Genome Inf.* 15, 138–148.
- Lahav, G., Rosenfeld, N., Sigal, A., Geva-Zatorsky, N., Levine, A., Elowitz, M., Alon, U., 2004. Dynamics of the p53-mdm2 feedback loop in individual cells. *Nat. Gen.* 36, 147–150.
- Lee, E., Boone, D., Chai, S., Libby, S., Chien, M., Lodolce, J., Ma, A., 2000. Failure to regulate TNF-induced NF- κ B and cell death responses in A20-deficient mice. *Science* 289 (5488), 2350–2354.
- Lipniacki, T., Paszek, P., Brasier, A.R., Luxon, B., Kimmel, M., 2004. Mathematical model of NF- κ B regulatory module. *J. Theor. Biol.* 228, 195–215.
- Lomakin, A., Nadezhdina, E., 2010. Dynamics of nonmembranous cell components: role of active transport along microtubules. *Biochemistry (Mosc)* 75, 7–18.
- Mackenzie, G., Keen, C., Oteiza, P., 2006. Microtubules are required for NF- κ B nuclear translocation in neuroblastoma IMR-32 cells: modulation by zinc. *J. Neurochem.* 99, 402–415.
- Matsuda, T., Miyawaki, A., Nagai, T., 2008. Direct measurement of protein dynamics inside cells using a rationally designed photoconvertible protein. *Nat. Methods* 5, 339–345.
- Meyers, J., Craig, J., Odde, D., 2006. Potential for control of signaling pathways via cell size and shape. *Curr. Biol.* 16, 1685–1693.
- Mikenberg, I., Widera, D., Kaus, A., Kaltschmidt, B., Kaltschmidt, C., 2007. Transcription factor NF- κ B is transported to the nucleus via cytoplasmic dynein/dynactin motor complex in hippocampal neurons. *PLoS ONE* 2 (7), e589.
- Monk, N., 2003. Oscillatory expression of Hes1, p53, and NF- κ B driven by transcriptional time delays. *Curr. Biol.* 13, 1409–1413.
- Nair, A., Venkatraman, M., Maliekal, T., Nair, B., Karunagaran, D., 2003. NF- κ B is constitutively activated in high-grade squamous intraepithelial lesions and squamous cell carcinomas of the human uterine cervix. *Oncogene* 22, 50–58.
- Nelson, D., Ihekwaba, A., Elliott, M., Johnson, J., Gibney, C., Foreman, B., Nelson, G., See, V., Horton, C., Spiler, D., Edwards, S., McDowell, H., Unitt, J., Sullivan, E., Grimley, R., Benson, N., Broomhead, D., Kell, D., White, M., 2004. Oscillations in NF- κ B signaling control the dynamics of gene expression. *Science* 306, 704–708.
- Neves, S., Tsokas, P., Sarkar, A., Grace, E., Rangamani, P., Taubenfeld, S., Alberini, C., Schaff, J., Blitzer, R., Moraru, I., Iyengar, R., 2008. Cell shape and negative links in regulatory motifs together control spatial information flow in signaling networks. *Cell* 133, 666–680.
- Pando, M., Verma, I., 2000. Signal-dependent and -independent degradation of free and NF- κ B-bound I κ B α . *J. Biol. Chem.* 275, 21278–21286.
- Park, J., Kim, K., Kim, M., Chang, H., Baek, M., Kim, S., Jung, Y., 2009. Resveratrol inhibits tumor cell adhesion to endothelial cells by blocking ICAM-1 expression. *Anticancer Res.* 29, 355–362.
- Perkins, N., 2007. Integrating cell-signalling pathways with NF- κ B and IKK function. *Nat. Rev. Mol. Cell Biol.* 8, 49–62.
- Pigolotti, S., Krishna, S., Jensen, M., 2007. Oscillation patterns in negative feedback loops. *Proc. Natl. Acad. Sci. USA* 104, 6533–6537.
- Pommier, Y., Sordet, O., Antony, S., Hayward, R., Kohn, K., 2004. Apoptosis defects and chemotherapy resistance: molecular interaction maps and networks. *Oncogene* 23, 2934–2949.
- Puszynski, K., Bertolusso, R., Lipniacki, T., 2009. Crosstalk between p53 and NF- κ B systems: pro- and anti-apoptotic functions of NF- κ B. *IET Syst. Biol.* 3, 356–367.
- Ribbeck, K., Gorlich, D., 2001. Kinetic analysis of translocation through nuclear pore complexes. *EMBO J.* 20, 1320–1330.
- Rice, N., Ernst, M., 1993. In vivo control of NF- κ B activation by I κ B α . *EMBO J.* 12, 4685–4695.
- Sachdev, S., Hoffmann, A., Hannink, M., 1998. Nuclear localization of I κ B α is mediated by the second ankyrin repeat: the I κ B α ankyrin repeats define a novel class of cis-acting nuclear import sequences. *Mol. Cell Biol.* 18, 2524–2534.
- Schrider, D., Hahn, M., 2010. Gene copy-number polymorphism in nature. *Proc. Roy. Soc. B* 277, 3213–3221.
- Seksek, O., Biwersi, J., Verkman, A.S., 1997. Translational diffusion of macromolecule-sized solutes in cytoplasm and nucleus. *J. Cell Biol.* 138, 131–142.
- Song, H., Rothe, M., Goeddel, D., 1996. The tumor necrosis factor-inducible zinc finger protein A20 interacts with TRAF1/TRAF2 and inhibits NF- κ B activation. *Proc. Natl. Acad. Sci. USA* 93, 6721–6725.
- Sturrock, M., Terry, A., Xirodimas, D., Thompson, A., Chaplain, M., 2011. Spatio-temporal modelling of the Hes1 and p53-Mdm2 intracellular signalling pathways. *J. Theor. Biol.* 273, 15–31.
- Sun, S.C., Ganchi, P., Ballard, D., Greene, W., 1993. NF- κ B controls expression of inhibitor I κ B α : evidence for an inducible autoregulatory pathway. *Science* 259, 1912–1915.
- Terry, A., Sturrock, M., Dale, J., Maroto, M., Chaplain, M., 2011. A spatio-temporal model of Notch signalling in the zebrafish segmentation clock: conditions for synchronised oscillatory dynamics. *PLoS ONE* 6 (2), e16980.
- Tiana, G., Krishna, S., Pigolotti, S., Jensen, M., Sneppen, K., 2007. Oscillations and temporal signalling in cells. *Phys. Biol.* 4, R1–R17.
- Wawra, C., Kuhl, M., Kestler, H.A., 2007. Extended analyses of the Wnt/ β -catenin pathway: robustness and oscillatory behaviour. *FEBS Lett.* 581, 4043–4048.
- Weinberg, R., 2007. *The Biology of Cancer*. Garland Science, Taylor & Francis Group.
- Werner, S., Kearns, J., Zadorozhnaya, V., Lynch, C., O’Dea, E., Boldin, M., Ma, A., Baltimore, D., Hoffmann, A., 2008. Encoding NF- κ B temporal control in response to TNF: distinct roles for the negative regulators I κ B α and A20. *Genes Dev.* 22, 2093–2101.